1 # Establishing Probiotic *Saccharomyces boulardii* as a Model
2 Organism for Synthesis and Delivery of Biomolecules

3

4 Deniz Durmusoglu[1,†], Ibrahim Al'Abri[1,†], Scott P. Collins[1], Chase Beisel[1], Nathan
5 Crook[1*]

6
7 [1]Department of Chemical and Biomolecular Engineering, North Carolina State University, Raleigh, North

8 Carolina, USA.

9 [†]These authors contributed equally to this work

10 [*]To whom correspondence should be addressed: nccrook@ncsu.edu

11

Abstract

Saccharomyces boulardii is a widely used yeast probiotic which can counteract various gastrointestinal disorders[1]. As a relative of *Saccharomyces cerevisiae*, *S. boulardii* exhibits rapid growth and is easy to transform[2] and thus represents a promising chassis for the engineered secretion of biomolecules. To establish *S. boulardii* as a platform for delivery of biomolecules to the mammalian gut, we measured the amount and variance in protein expression enabled by promoters, terminators, selective markers, and copy number control elements in this organism. These genetic elements were characterized in plasmidic and genomic contexts, revealing strategies for tunable control of gene expression and CRISPR-mediated genome editing in this strain. We then leveraged this set of genetic parts to combinatorially assemble pathways enabling a wide range of drug and vitamin titers. Finally, we measured *S. boulardii*'s residence time in the gastrointestinal tracts of germ-free and antibiotic-treated mice, revealing the relationships between dosing strategy and colonization level. This work establishes *S. boulardii* as a genetically tractable commensal fungus and provides a set of strategies for engineering *S. boulardii* to synthesize and deliver biomolecules during gut colonization.

Introduction

29   Next-generation probiotics offer unique attributes for the delivery of biomolecules to the gut[3].

30   By leveraging decades of work in metabolic engineering[4], engineered probiotics have enabled

31   the conversion of unused dietary material to beneficial products for the host[5–7]. Furthermore,

32   the ongoing development of synthetic biological sensors advance the concept of drug synthesis

33   tailored to the severity and location of disease within the host[8–11]. Coupled with existing

34   manufacturing expertise in food science and infrastructure in place for distributing probiotics,

35   engineered probiotics promise to substantially reduce the costs associated with production of

36   drug molecules[12]. All engineered probiotics described to date have been members of the

37   bacterial domain of life due to their high numerical abundance in the gut[13,14] and ease of

38   engineering.[9,15] For example, *Escherichia coli* Nissle 1917 has been engineered to treat diseases

39   such as phenylketonuria (PKU)[15,16], hyperammonemia[17], and cancer[18], or eliminate pathogens

40   such as *Pseudomonas aeruginosa*[19]. In addition to these advantages, the limitations to bacterial

41   probiotics include susceptibility to antibiotics,[20] predation by bacteriophage known to be highly

42   abundant in the human gut,[21] and difficulty in producing high levels of post-translationally-

43   modified proteins[22].

44

45   In addition to bacteria, a diverse fungal population also exists in the human gastrointestinal tract

46   (GIT)[23–26]. While the numerical abundance of fungal cells in the GIT is much lower than bacterial

47   cells, fungal cells are on average 100-fold larger, indicating that their biomass and role in the gut

48   may be larger than metagenomic surveys indicate[25,27]. Recent studies have shown that while

49   commensal fungi play important roles in the development of inflammatory bowel diseases, they

50   also provide protective heterologous immunity to pathogenic organisms by training the immune

51   system[28,29]. Furthermore, fungi are not susceptible to bacteriophage predation and are easily

52   engineered to secrete high titers of proteins that are post-translationally modified. Thus, in this

53   study, we established a pipeline to engineer the only eukaryotic probiotic that is approved by the

54   FDA: *Saccharomyces boulardii*[30].

55

56   *S. boulardii* is a non-pathogenic yeast that was originally isolated from lychee and mangosteen in

57   1923 and has since been used to treat ulcerative colitis, diarrhea, and recurrent *Clostridium*

58   *difficile* infection[1,31]. *S. boulardii* is closely related to the famous budding yeast *Saccharomyces*

59   *cerevisiae*, indicating that it may be similarly amenable to engineering for the production of

60   biomolecules, including biologics requiring post-translational modifications[2,32]. Supporting this,

61   *S. cerevisiae* expression vectors can be transformed and propagated in *S. boulardii*, and

62   CRISPR/Cas9-mediated genome editing is functional in both strains[33]. However, compared to *S.*

63   *cerevisiae, S. boulardii* better tolerates low pH environments and grows more rapidly at human

64   body temperature[32,34,35]. Given its regulatory status, genetically tractability, and well-studied

65   yeast relative, *S. boulardii* is uniquely poised as a potential model chassis for the delivery of

66   therapeutics to the human gut. Indeed, *S. boulardii* has been engineered to secrete human

67   synthetic lysozyme[33] and HIV-1 Gag[36] in cell culture, as well as IL-10 in an IBD mouse model[37].

68   However, while the rules governing high-level biomolecule production in *S. cerevisiae* have been

69   extensively studied, these rules remain to be defined in culture- and gut-resident *S. boulardii*. In

70   this work, we sought to develop a quantitative framework for engineering *S. boulardii* for *in situ*

71 production and delivery of therapeutics to the mammalian gut. We began by assaying the ability

72 of a library of *S. cerevisiae* genetic parts[38] to drive gene expression from various plasmidic and

73 genomic contexts in *S. boulardii*. We then applied these genetic parts to rapidly construct and

74 identify *S. boulardii* strains exhibiting high levels of vitamin (β-carotene) or drug (violacein)

75 production. Finally, we measured the residence time of *S. boulardii* in the mouse gut. Taken

76 together, this work demonstrates the promise of, and details a set of procedures for engineering,

77 *S. boulardii* for producing biomolecules in the gut.

78

79 # Results

80 **Selective marker and plasmid origin tune gene expression over a wide range in *S.***

81 ***boulardii***

82 Plasmids enable rapid prototyping of synthetic constructs in many organisms, including yeast.

83 The tunability of gene expression on plasmids is due in part to plasmid-specific copy number

84 control sequences, which in yeast have been shown to include the origin of replication (origin)

85 and selectable marker (marker)[39]. We therefore first sought to understand the interplay between

86 origin and marker in determining the expression of a model fluorescent reporter gene. An

87 optimal reporter gene, when expressed, should yield detection signals well above the

88 background signal produced by non-expressing strains in order to precisely resolve gene

89 expression levels[40]. Therefore, we first measured the cell fluorescence conferred by three

90 proteins (*Venus, mTurquoise2, mRuby2*) when expressed by the *TDH3* promoter and the *TDH1*

91   terminator on a plasmid harboring a *URA3* marker and the 2μ origin. Fluorescence levels were

92   measured at log phase using flow cytometry. In all experiments, we normalized the resulting

93   fluorescence levels to those of a strain harboring an empty vector. *Venus* displayed the highest

94   normalized fluorescence (1080-fold) (Supplementary Figure S1). However, *Venus* fluorescence

95   also exhibited high cell-to-cell variability compared to that for *mRuby2* and *mTurquoise2*, and its

96   fluorescence distribution was non-gaussian, suggesting that *Venus* would not be suitable for

97   measuring fine differences in expression. On the other hand, *mRuby2* showed the second highest

98   normalized fluorescence (450-fold) and exhibited a more gaussian fluorescence distribution.

99   Because *mRuby2* exhibited a 2.6-fold higher normalized fluorescence than *mTurquoise2*, we

100 decided to proceed with *mRuby2* for further analysis of synthetic construct performance in *S.*

101 *boulardii*.

102

103 We generated expression cassettes containing the *TDH3* promoter (*pTDH3*), *mRuby2*, and the

104 *TDH1* terminator (*tTDH1*) in combination with 3 auxotrophic markers (*URA3*, *HIS3* and *TRP1*) or

105 four antifungal markers (geneticin resistance (*KanMX*), zeocin resistance (*ZeoR*), nourseothricin

106 resistance (*NatR*), and hygromycin resistance (*HygR*)) and two origins-of-replication (CEN6/ARS4

107 (*CEN*, low-copy) and 2-micron (2μ, high-copy)). We transformed the cassettes containing

108 auxotrophic markers into corresponding auxotrophic strains (*S.bΔURA3*, *S.bΔHIS3* and *S.bΔTRP1)*

109 and antifungal markers into wild-type strain. We achieved a maximum normalized fluorescence

110 of 400 using *URA3* and 2μ (Figure 1a, Supplementary Figure S2a). Among antifungal markers,

111 *HygR* coupled with the 2μ origin yielded the highest fluorescence (Figure 1a). Other

112 marker/origin combinations yielded a 100-fold variation in fluorescence (Figure 1a,

113 Supplementary Figure S2). This large range in expression levels for constructs containing the

114 same promoter and terminator indicated that, as in *S. cerevisiae*, plasmid origin and marker have

115 significant effects on gene expression in *S. boulardii*.

116

The impact of origin on gene expression is marker-dependent in *S. boulardii*.

118 We next asked whether certain markers or origins had consistent effects on fluorescence. For

119 auxotrophic markers, 2μ plasmids consistently yielded higher fluorescence than CEN plasmids

120 (Two-way ANOVA, $p < 0.05$) (Figure 1a). This is consistent with prior work in *S. cerevisiae*, which

121 demonstrated that 2μ plasmids with auxotrophic markers are maintained at 28-58 copies per

122 cell, whereas CEN plasmids are maintained at only 4-8 copies per cell[39]. However, with the

123 exception of *HygR* (Two-way ANOVA, $p < 0.0001$), the fluorescence conferred by plasmids

124 containing antifungal markers was not impacted by the choice of origin (Two-way ANOVA,

125 $p > 0.05$). For the CEN origin, using *NatR* at the maximum antifungal concentration yielded the

126 highest fluorescence level. This level was significantly higher expression than those conferred by

127 the *HIS3*, *ZeoR*, *KanMX*, or *HygR* markers (Two-way ANOVA, $p < 0.05$). However, for the 2μ origin,

128 using any of the auxotrophic markers gave gene expression levels higher than any antifungal

129 marker (Two-way ANOVA, $p < 0.0001$). Taken together, our data indicate that gene expression

130 conferred by plasmids containing auxotrophic markers (but not antifungal markers) is sensitive

131 to the choice of origin, and that selective marker significantly impacts gene expression for both

132 2μ and CEN origins.

133

Plasmidic gene expression noise is marker and origin dependent in *S. boulardii*

Cell-to-cell variability in gene expression can have dramatic impacts on overall production titers[41]. Therefore, it is desirable to design engineered probiotics to exhibit minimal gene expression noise. Previous work characterizing gene expression noise in *S. cerevisiae* showed that cell variability varies as a function of promoter, terminator, origin, and selective marker[42]. We thus calculated the population-level coefficient of variance (CV) in the fluorescence values we obtained for *S. boulardii*. We found that marker, origin, and marker-origin interactions had significant impacts on expression noise (Two-way ANOVA, $p<0.05$). Specifically, CEN plasmids exhibited less cell-cell variability than 2μ plasmids (Two-way ANOVA, $p<0.05$). Additionally, antifungal markers exhibited less noisy expression than auxotrophic markers (Two-way ANOVA, $p<0.05$). These data suggest differences in the ways that the auxotrophic and antifungal markers interact with origins of replication to control gene expression, and point to design strategies which reduce plasmid-based gene expression variance.

S. cerevisiae **promoters largely maintain their relative activities in *S. boulardii*.**

Promoter sequences are frequently employed to tune the expression of individual genes in yeast[43,44]. Here, we quantified the transcriptional strength of 18 constitutive *S. cerevisiae* promoters driving the expression of a fluorescent protein in *S. boulardii*. Each of these promoters had a homolog in *S. boulardii*, with percent nucleotide identities ranging from 100% to 97% (Supplementary Table S1). In these experiments, vectors contained the 2μ origin and the *URA3* auxotrophic marker, which maximized the range over which changes to fluorescence could be detected (Figure 1a). Each promoter drove the expression of *mRuby2* and transcription was

156   terminated by *tTHD1*. These constructs were transformed into *S. boulardii* and fluorescence

157   levels were measured at log phase via flow cytometry. Each promoter yielded different mean

158   fluorescence values (Two-way ANOVA, p<0.0001), and these promoters collectively modulated

159   fluorescence levels over a 40-fold range (Figures 1b, S3). While the relative activities of 17 of the

160   18 promoters in *S. boulardii* were similar to reported values in *S. cerevisiae* , one promoter

161   (*pALD6*) showed 10-fold higher activity in *S. boulardii* than in *S. cerevisiae* (Supplementary Figure

162   S4). While the precise role of *ALD6* in the probiotic properties of *S. boulardii* is unknown, Ald6p

163   is involved in the detoxification of aldehyde molecules to their corresponding acid in *S.*

164   *cerevisiae*[45]. Collectively, this data curates a set of promoters enabling precise tuning of gene

165   expression in *S. boulardii*, and indicates that constructs developed for *S. cerevisiae* will exhibit

166   similar gene expression profiles in *S. boulardii.*

167

168   **Terminators modulate gene expression in a promoter-dependent manner in *S.***

169   ***boulardii***

170   Terminators regulate expression in yeast by modulating mRNA stability, translational efficiency

171   and mRNA localization[46]. Furthermore, a terminator's effect on expression can depend on the

172   strength of the promoter or the sequence of the expressed gene[47,48]. Therefore, we were

173   interested in defining the effect of terminator choice on gene expression in *S. boulardii*. We

174   cloned 6 terminators (*tENO1, tENO2, tSSA1, tPGK1, tADH1,* and *tTDH1*) into mRuby2 expression

175   constructs driven by strong (*pTDH1*), medium (*pRNR1*), or weak (*pREV1*) promoters. We found

176   that these terminators could modulate gene expression by 1.77, 1.81, and 1.64-fold in constructs

177   containing *pTDH1*, *pRNR1*, or *pREV1*, respectively, effectively increasing the expression range

178 beyond that enabled by varying the promoter alone (40-fold, Figure 1b). In particular, using a

179 strong promoter (*TDH3*) with the *TDH1* terminator yielded 80-fold higher expression than a weak

180 promoter (*REV1*) with the *SSA1* terminator. Relative to *tSSA1 and tTDH1,* we found that *tENO1,*

181 *tENO2, tADH1* and *tPGK1* significantly decreased gene expression in constructs containing the

182 strong *pTDH3* promoter (Two-way ANOVA, $p < 0.005$) while for *pRNR1* and *pREV1*, the differences

183 in gene expression we observed among terminators were not statistically significant (Two-way

184 ANOVA, $p > 0.05$) (Figure 1c, S5). Taken together, this data suggests that varying the terminator is

185 a valuable way to fine-tune gene expression, particularly when certain regulatory characteristics

186 of the promoter (e.g. responsiveness to growth phase or gut conditions) must be maintained.

187

188 **The *S. boulardii* genome can be efficiently modified by CRISPR-Cas genome**

189 **editing**

190 Genomic integration of synthetic constructs can sidestep issues associated with the use of

191 plasmids in the gut. Such issues include plasmid instability if no selective pressure is present,

192 potential spread to other microbes, collateral damage to the microbiota if antimicrobials are used

193 to select for plasmid maintenance, and the increased metabolic burden associated with the

194 maintenance of multicopy plasmids. However, different genomic regions are known to support

195 varying levels of synthetic construct expression, potentially due to nucleosome positioning[49], and

196 integrating material into the genome can be especially difficult for diploid and polyploid

197 organisms[50].

198

199   To characterize and overcome inefficiencies associated with genome integration, we compared

200   three different editing methods in *S. boulardii*: un-assisted linear dsDNA integration (dsDNA

201   integration) and genome editing assisted with the CRISPR nucleases SpCas9 or LbCas12a . We

202   tested the ability of these methods to integrate a linear expression cassette containing

203   *mTurquoise2* in three different loci (INT1, 4 and 5) via colony PCR. In the case of dsDNA

204   integration, 4/12 transformants did not contain the expected *mTurquoise2* insertion, while 7/12

205   colonies yielded multiple PCR fragments (Supplementary Figure S6). Sequencing revealed that

206   the larger fragment corresponded to the desired integration, while the shorter fragment

207   corresponded to the native genomic locus. This result is likely due to the fact that the *S. boulardii*

208   genome is diploid, and that integration of one copy of the construct is sufficient to confer uracil

209   prototrophy.. Therefore, we tested whether CRISPR-based editing tools could achieve more

210   complete genome editing in *S. boulardii*. We reasoned that since CRISPR-Cas systems enhance

211   the proportion of double-stranded breaks in all copies of the targeted sequence, editing of all

212   chromosomal copies would be a preferred survival strategy. Three sgRNAs for SpCas9 and three

213   gRNAs for LbCas12a were designed for each integration site. Targeted loci were followed by a 5'-

214   NGG-3' protospacer adjacent motif (PAM) for SpCas9 and preceded by a 5'-TTTV-3' PAM (V = A,

215   C, G) for LbCas12a. Supplementary Figure S7c-f shows the plasmid designs we used for CRISPR-

216   based editing, Supplementary Table S2 shows integration locations (INT1-INT5) in *S. boulardii*'s

217   genome, and Supplementary Table S3 shows the guide RNA sequences we used.

218

219   We tested the editing efficiency at each integration site (using a single guide RNA per experiment)

220   as above for un-assisted linear DNA integration. Supplementary Table S4 shows the number of

221   fluorescent colonies we observed for each editing method. Colony PCR of 4 random fluorescent

222   transformants from each experiment revealed a single band corresponding to either the edited

223   or the unedited version of the locus (Supplementary Figure S8). Altogether, we were able to

224   generate genome integrants with 82-88% efficiency for SpCas9 and 93-99% efficiency for

225   LbCas12a in *S. boulardii* (Figure 2a, Supplementary Table S4). Thus, these results indicate that

226   CRISPR/LbCas12a-assisted genome editing has >10% and >50% higher editing efficiency than

227   CRISPR/SpCas9 and dsDNA integration, respectively, and is therefore a promising choice for

228   future editing in this strain.

229

230   **Integration locus has a minor effect on gene expression, relative to promoter**

231   **choice**

232   To determine the extent of locus-dependent effects on gene expression in *S. boulardii*, we

233   integrated constructs driving *mRuby2* or *mTurquoise2* expression into five different locations in

234   the *S. boulardii* genome (Supplementary Table S2) using LbCas12a. These genes were regulated

235   by *pTDH3* and *tTDH1*, and constructs contained *URA3* to select for edited strains (Supplementary

236   Figure S7b). The *mRuby2* and *mTurquoise2* fluorescent proteins are sequence-divergent, with

237   only 30% amino acid identity. These two proteins therefore enabled a cursory view into the

238   generalizability of these patterns across genes. Across integration sites, the expression of

239   *mRuby2* and *mTurquoise2* varied 3.4-fold and 2.6-fold, respectively (Figure 2b, S9). INT2

240   supported the lowest expression for both genes, while INT4 supported the highest expression

241   levels for *mRuby2* and INT5 supported the highest expression level for *mTurquoise2*. We next

242   asked whether differences in promoter strength observed in the plasmid-based system would be

11

243 similar for genomically-integrated constructs. We therefore expressed *mRuby2* and *mTurquoise2*

244 from two additional promoters in INT4: *pRNR1* and *pREV1*. Intriguingly, genomic *mRuby2*

245 expression varied by 5.9-fold between *pTDH3* and *pRNR1*, compared with 2.8-fold for the same

246 construct on a 2μ plasmid. Conversely, genomic *mRuby2* expression varied by 15.3-fold between

247 *pTDH3* and *pREV1*, compared to 31.2-fold for the same promoters used on a 2μ plasmid (Figure

248 2c). This could indicate that gene expression from high-copy plasmids saturates at high promoter

249 strengths, or that promoter strength varies with copy number due to transcription factor dilution.

250 Together, this work establishes a pipeline for efficient genome integration in *S. boulardii* and

251 identifies regions of the *S. boulardii* genome enabling high-level expression of synthetic

252 constructs. Further, these data show that the impact of integration locus on gene expression is

253 relatively small in *S. boulardii* compared to that of the promoter.

254

255 ***S. boulardii* facilitates high-throughput metabolic engineering through *in vivo***

256 **combinatorial assembly of multi-enzyme pathways**

257 Having found that *S. boulardii* could support genome integration via homologous recombination,

258 we asked if recombination efficiencies were sufficient for *in vivo* assembly of biosynthetic

259 pathways. In *S. cerevisiae,* combinatorial *in vivo* assembly is a facile technique for rapid

260 optimization of metabolic pathways[51–53]. Large scale assembly of common heterologous

261 metabolic pathways directly in *S. boulardii* would simplify strain development and might reveal

262 the potential for *S. boulardii* as a host for biomolecule production.

263

264 We implemented golden gate assembly to streamline *in vivo* assembly workflows in *S. boulardii*.

265 Namely, we started from our characterized promoter, coding sequence (CDS), and terminator

266 parts and assembled pathways directly in yeast with minimal subcloning (Figure 3a). Our

267 assembly strategy involved two steps: a golden gate assembly step to assemble a 9-member

268 gene-level library of promoter-CDS-terminator transcriptional units for each gene in the pathway

269 of interest and *in vivo* homologous recombination to assemble the gene-level libraries created in

270 step 1 into pathways, as shown in Figure 3a. Each gene-level library member differed only in the

271 promoter driving gene expression. These transcriptional units are flanked with homology arms

272 which facilitate *in vivo* assembly. These gene-level libraries are then PCR-amplified directly from

273 the Golden Gate reaction mixture. Purified amplicons are transformed into *S. boulardii,* where

274 flanking sequences direct homology-dependent assembly of the final pathway with one variant

275 of each transcriptional unit. We used this method to construct β-carotene and violacein synthesis

276 pathways, which provided a direct colorimetric readout of assembly efficacy (Supplementary

277 Figures S10a and S10b). Supplementary Figures S10c and S10d show spotted cultures of 28 library

278 members from the β-carotene pathway and 24 library members from the violacein pathway.

279 Colony sequencing revealed that each strain harbored a plasmid containing the expected

280 pathway topology, with each gene driven by one of the 10 selected promoters and the desired

281 terminator.

282

283 We next focused on those strains exhibiting qualitatively stable pigment levels over three rounds

284 of growth of solid media. 13 out of 28 strains and 8 out of 24 strains stably produced β-carotene

285 and violacein molecules, respectively. We determined the identity of the promoters driving each

286   gene in these strains. We also quantified the amount of β-carotene produced by these strains to

287   understand how different combinations of promoters regulate biomolecule production. Figures

288   3b and S11 show the strength of the promoters comprising each assembled pathway and amount

289   of β-carotene or violacein produced by each assembled pathway. Interestingly, we found that

290   strains with the highest qualitative color intensity and quantitative β-carotene concentration did

291   not harbor strong promoters for all the genes in the pathway. In fact, many high producers

292   contained moderate or low-strength promoters in at least one of their genes. Additionally, we

293   observed cases where multiple pathway genes in a high-producing strain were driven by the

294   same promoter. This suggests that product titers in these strains were not sufficiently high to

295   select for the emergence of non-producers via homologous recombination.

296

297   The optimal expression levels for several genes in the β-carotene are not obvious from the

298   biosynthetic reaction map[54]. *HMG1* diverts flux from cellular acetyl-coA pools into the β-carotene

299   pathway, thereby reducing the amount of acetyl-coA available for other processes. *crtYB* can

300   convert lycopene into the desired product β-carotene, but can also convert neurosporene (a

301   precursor to lycopene) into the side product 7,8-dihydro-β-carotene (β-zeacarotene). *crtI*

302   operates on several pathway intermediates, including phytoene, ζ-carotene, and

303   neurosporene[55]. Figure 3b shows substantial variations in β-carotene titer depending on the

304   expression level of these genes. As complex tradeoffs between gene expression and pathway

305   output will likely also be present in engineered strains colonizing the gut, combinatorial assembly

306   is useful for rapidly generating strain designs for subsequent *in vivo* testing or screening. Our

307   results reveal that high biomolecule titers can be achieved via expression tuning, confirming

308 previous results from other methods for pathway optimization in *S. cerevisiae*[52,53,56]. Moreover,

309 as in *S. cerevisiae*, large combinatorial pathway libraries can be easily generated in *S. boulardii*,

310 enabling rapid optimization of biomolecule titers.

311

The Mouse Microbiota Restricts *S. boulardii* Colonization

313 Host immunity, intestinal peristalsis, inter-microbial competition, and nutrient availability shape

314 the residence time of microbes in the gut. To parse this complexity, gnotobiotic mouse models

315 are attractive to explore the behavior of microbes in defined gut ecologies. Thus, we first

316 measured *S. boulardii's* residence time in the germ-free gut by delivering *S. boulardii* (10^8, 10^7, or

317 10^6 colony-forming units) to germ-free mice via oral gavage (Supplementary Figure S12). No

318 deleterious effects on mouse health were apparent during the experiment. While all dosages

319 yielded similar fecal loads of *S. boulardii* through day 5 (3×10^6 CFU/g feces), we found that when

320 mice were provided at least 10^8 CFUs, consistent fecal loads of 10^7 CFU/g *S. boulardii* were

321 maintained for over 30 days. On the other hand, mice gavaged with 10^6 and 10^7 CFUs showed 3-

322 fold lower fecal titers starting on day 7. Thus, the initial dose of *S. boulardii* impacts its fecal titer

323 and residence time in germ-free mice. Furthermore, in the absence of microbial competitors, *S.*

324 *boulardii* is capable of long-term (>30 days) colonization of the GIT.

325

326 We next asked whether the presence of microbial competitors would modulate the gut residence

327 time of *S. boulardii*. To answer this, we turned to conventionally-raised mice treated with

328 antibiotics[57]. In these experiments, we were initially unable to track *S. boulardii* titers via plating

329 because other native gut fungi outgrew *S. boulardii* on YPD plates containing 0.125 mg/ml

15

330   penicillin and 0.25 mg/ml streptomycin. Therefore, we hypothesized that integration of an

331   antifungal resistance gene into the *S. boulardii* genome would allow easier identification via

332   plating on media containing antifungals. Based on the observed minimum inhibitory

333   concentrations (MICs) of various antifungals against *S. boulardii* (Supplementary Figure S13), we

334   integrated the nourseothricin resistance gene (*NatR*) into the *S. boulardii* genome. We found that

335   NatR-containing *S. boulardii* was the only microbe from mouse feces able to grow on YPD plates

336   containing 50 µg/ml nourseothricin, 0.125 mg/ml Penicillin and 0.25 mg/ml streptomycin (data

337   not shown). We then provided conventional mice with 1mg/ml penicillin and 2mg/ml

338   streptomycin in their drinking water for four days, after which antibiotics treatment ceased and

339   10^8 CFU of *S. boulardii* was delivered once per day for three days. Under this regimen (Treatment

340   1, Figure 4b), we found that *S. boulardii* titers fell to undetectable levels within 48 hours of the

341   last gavage (Figure 4D). On the other hand, when antibiotic treatment was maintained over the

342   course of the experiment (Treatment 2, Figure 4c), the titer and residence time of *S. boulardii*

343   both increased, enabling *S. boulardii* to remain present in the gut one additional day after the

344   last gavage (Figure 4D). These results are in line with previous *S. boulardii* colonization studies

345   performed in mice colonized by a human microbiota[58]. Taken together, these experiments

346   indicate that competitive microbial growth reduces the residence time of *S. boulardii* in the

347   mouse gut. In these contexts, *S. boulardii*-mediated drug delivery will only occur during and for

348   several days after probiotic administration, thereby minimizing dosage outside of desired

349   therapeutic timescales.

350

16

Conclusion

351

352 The gut and the microbes that live within it play a major role in host health, and as such are

353 promising targets for manipulation via small molecule or biologic drugs. Unfortunately, delivering

354 drugs to this environment remains challenging due to the digestive action of the host, especially

355 for protein-based therapies. Due to its probiotic properties and similarity to the

356 biomanufacturing workhorse organism *S. cerevisiae*, we characterized the ability of *S. boulardii*

357 to be engineered to secrete biomolecules in the mammalian gut. We first characterized the effect

358 of different plasmid-based and genomic sequences on the expression of synthetic constructs. We

359 next established efficient genome editing tools for this strain and revealed the effects of genomic

360 integration site on synthetic construct performance. We further harnessed *S. boulardii*'s high

361 rates of homologous recombination to combinatorially assemble pathways for vitamin (β-

362 carotene) and drug (violacein) production. Finally, we measured *S. boulardii*'s residence time in

363 germ-free and antibiotic-treated mice. Taken together, these results indicate that the decades of

364 work developing *S. cerevisiae* as a platform for biomanufacturing and synthetic biology can be

365 readily extended to *S. boulardii*. Coupled with the continued development of engineered

366 commensal and probiotic bacteria, *in situ* biomanufacturing by gut-resident microbes has the

367 potential to greatly reduce distributional complexity, improve site-specific delivery, and reduce

368 production costs for a wide array of biomolecules.

369

Acknowledgments

Methods

Strains and Culture Media

Escherichia coli Top10, NEB 5α and NEB 10β were used for plasmid construction and maintenance. *E. coli* cells were grown in lysogeny broth (LB) (5g/L yeast extract, 10 g/L tryptone, 10 g/L NaCl) at 37 °C supplemented with ampicillin (100 µg/mL), kanamycin (50 µg/mL) or chloramphenicol (50 µg/mL). *Saccharomyces boulardii* ATCC-MYA796 was used for antifungal marker and origin of replication characterization. *Saccharomyces boulardii ΔURA3,* provided by

18

389 Yong-Su Jin, was used for auxotrophic marker, origin of replication, promoter, and terminator

390 characterization, as well as genome editing and metabolic pathway assembly. *Saccharomyces*

391 *boulardii* ΔTRP1 and ΔHIS3 strains from the Jin Lab were used for auxotrophic marker and origin

392 of replication characterization. Promoter and terminator characterization experiments were

393 conducted in synthetic media containing 0.67% (w/v) Yeast Nitrogen Base Without Amino Acids

394 (Sigma-Aldrich), 2% Glucose (Fisher Scientific), 1.92g/L Yeast Synthetic Media Drop-Out Mix

395 without Uracil (Sigma-Aldrich). For auxotrophic marker characterization, synthetic media with

396 0.67% (w/v) Yeast Nitrogen Base Without Amino Acids (Sigma-Aldrich), 2% Glucose (Fisher

397 Scientific), 1.92% Yeast Synthetic Media Drop-Out Mix without the appropriate nutrient

398 (histidine, tryptophan, or uracil) (Sigma-Aldrich) was used. Antifungal marker characterization

399 experiments were conducted in yeast extract-peptone-dextrose medium (50 g/L YPD broth

400 (Sigma-Aldrich)) supplemented with various concentrations (50 µg/mL, 100 µg/mL and 200

401 µg/mL) of geneticin (G418), zeocin, nourseothricin and hygromycin.

402

Plasmid Construction & Cloning

404 All plasmids used in this work are listed in Supplementary File S1. A synthetic toolkit (MoClo-YTK)

405 containing yeast parts were gifts from the Dueber Lab (Addgene #:1000000061). Characterization

406 plasmids consisted of 8 parts: 2 connectors, promoter, coding sequence, terminator, yeast

407 marker, yeast origin, and *E. coli* marker and origin. Each of these plasmids were assembled

408 according to Deuber lab YTK protocols via Golden Gate cloning[59]. The Golden Gate reaction

409 mixture, for all plasmids except those containing β-carotene or violacein pathways, was prepared

410 as follows: 0.5 µL of 40 nM of each YTK plasmid (20 fmol), 0.5 µL T7 Ligase (NEB) or 0.5 µL T4

411   Ligase (NEB), 1 µL T4 Ligase Buffer (NEB) and 0.5 µL BsaI (10000 U/mL, NEB) and water to bring

412   the final volume to 10 µL. The Golden Gate assembly protocol was performed on a thermocycler

413   with the following program: 30 cycles of digestion (42 °C for 2 minutes) and ligation (16 °C for 5

414   minutes), followed by a final digestion (60 °C for 10 minutes) and heat inactivation (80 °C for 10

415   minutes).

416

417   **Yeast Competent Cells and Transformations**

418   We optimized the yeast competent cell preparation and transformation protocol from Gietz et.

419   al for *Saccharomyces boulardii*[60,61]. For the characterization experiments, we used frozen

420   competent cells, whereas for the genome editing experiments we used unfrozen competent cells

421   prepared on the same day[60,61]. To prepare competent cells, yeast colonies were inoculated into

422   1mL YPD and incubated in a shaking incubator overnight at 37 °C, 250 rpm. This culture was

423   diluted into fresh 50 mL YPD (approximately OD_{600}=0.25), and grown for 6-8 hours until OD_{600}=1.

424   The culture was centrifuged at 3000 xg for 5 min at room temperature to pellet the cells. After

425   decanting the media, the pellet was resuspended in 25 mL of sterile water, and then pelleted at

426   3000 xg for 5 minutes. This pellet was resuspended in 1 mL of sterile water. The cells were then

427   pelleted down at 10000 xg for 1 minute and water was discarded. The cells were then

428   resuspended in 500 µL of frozen competent cell solution consisting of 2.5% (v/v) glycerol (Sigma-

429   Aldrich) and 5% (v/v) DMSO (Thermo-Fisher). 50 µL of this suspension was aliquoted into 1.5 mL

430   microcentrifuge tubes and stored in -80 °C. For transformations, frozen cells were thawed at 37 °C

431   for 1 minute. Then, the cells were pelleted by centrifugation at 3000 xg for 2 minutes, after which

432   the supernatant was removed. Then, solutions were added in the following order; 260 µL 50%

433   PEG3350 (Fisher Scientific), 36 µL 1M Lithium Acetate (Sigma-Aldrich), 50 µL of 2 mg/ml single-

434   stranded salmon sperm DNA ((Invitrogen™, 15632011) 10 mg/ml double-stranded salmon sperm

435   DNA was diluted to 2 mg/ml and heat treated at 95 °C for 5 minutes to denature the double-

436   stranded DNA), 0.1-10 µg DNA and water to bring the final volume to 360 µL. The pellet was

437   resuspended in the transformation mix by gently mixing with a pipette tip. This transformation

438   mix was incubated at 42 °C for one hour. This mixture was then centrifuged at 3000 xg for 1 min

439   and the supernatant was discarded. The cell pellet was resuspended in 1 mL YPD by gently

440   pipetting up and down and this tube was incubated at 37 °C for one hour. Then, the cell

441   suspension was centrifuged for one minute at 3000 xg, resuspended in 25 µL sterile water, and

442   plated on an appropriate growth media.

443

444   *S. boulardii* Colony PCR

445   Since *S. boulardii* has a thicker cell wall than *S. cerevisia*e, we developed a new method to

446   perform colony PCR on *S. boulardii*. Colonies were picked into 25 µL 20 mM sodium hydroxide

447   and incubated at 98 °C for 80 minutes. Then we centrifuged these reactions at max speed (Mini

448   Microcentrifuge Sargent-Welch) for 10 minutes and started a 25µL PCR reaction with 2µL of this

449   reaction as a template. Otherwise, PCR reactions were performed according to the supplier's

450   instructions.

451

452   **Flow Cytometry**

453   Constructs were inoculated from -80C freezer stocks into 750 µL of appropriate media in 96-

454   deep-well plates (VWR International) and incubated at 37 °C for 36 hours with shaking at 250

21

455   rpm. After 36 hours, the cultures were diluted 1:100 in 200 μL of fresh media in 96-well-plates

456   (Costar) and were grown for ~8-10 hours at 37 °C. Once the cultures reached OD_{600} values

457   between 0.1-0.4, flow cytometry was performed using a MACSQuant VYB (Miltenyi Biotec). Cells

458   containing empty vector were used as a control. The voltage of the channels were adjusted in

459   order to tune the gain of the detectors. The voltage values applied to FSC, SSC, Y1 (PE-A,

460   excitation:561, emission: 586/15 nm), V1 (CFP-VioBlue, excitation: 405 nm, emission: 450/50 nm)

461   and B1 (GFP_FITC, excitation: 488 nm, emission: 425/50 nm) channels/filters were 326V, 290V,

462   396V, 324V and 265V respectively. Flow cytometry data analysis was conducted on the FlowJo

463   program (FlowJo LLC). The mean fluorescence values obtained from the flow cytometry for each

464   transcriptional construct was then normalized to background fluorescence (i.e. the cells with an

465   empty vector).

466

467   **Mouse Experiments:**

468   All mouse experiments were approved by the NC State University Institutional Animal Care and

469   Use Committee (IACUC).

470   **Germfree Mice:**

471   6-10 week old male and female germ free C57BL/6 mice were born at the NCSU Gnotobiotic

472   Animal Core and were mono-colonized by *S. boulardii*. 2 mice (males) were gavaged with 10^6

473   colony forming units in 100 μL PBS, 8 mice (6 females and 2 males) were gavaged with 10^7 and 4

474   mice (2 females and 2 males) were gavaged with 10^8 *S. boulardii* cells on day 1 and fecal samples

475   were collected on days 2, 5 and 7. Fecal samples from mice housing the 10^8 inoculum were

476   collected on day 30.

22

477 **Conventional Mice:**

478 Six-week old female C57BL/6J mice were obtained from Jackson Labs and hosted at the NCSU

479 Biological Resources Facility (BRF) for 3-4 days before experiments. Mice were housed in groups

480 of three and their cages were changed before treatment with antibiotics and before treatment

481 with *S. boulardii* or water. All mice were treated with 1mg/ml penicillin and 2mg/ml streptomycin

482 in the drinking water for 4 days starting on day -3. On day 1, drinking water was either replenished

483 with antibiotic solution or changed to fresh water. Mice were then gavaged with 10^8 CFU *S.*

484 *boulardii* or water once every 24 hours for 3 days. Fecal samples were collected every 24 hours

485 from day 1 to day 5.

486 **Stool Cultures.**

487 1-2 pieces of stool were collected in weighed 1.5 ml centrifuge tubes and then weighed again to

488 determine fecal mass. Fecal matter was then resuspended in 1 mL PBS per 100 mg feces. Fecal

489 suspensions from mono-colonized mice were placed on solid YPD media, while fecal suspensions

490 from conventional mice treated with antibiotics were plated on YPD media containing 50 μg/ml

491 nourseothricin and 0.25 μg/ml streptomycin. Plates were sealed with parafilm and incubated at

492 37 °C for 2-3 days.

493

494 **Genome Editing:**

495 Integration plasmids contained *URA3* to aid selection and contained homology arms between

496 350 to 900 base-pairs in length as shown in Supplementary Figure S7. For DNA homologous

497 recombination without DSB (**dsDNA integration**), 2μg of linear donor DNA was transformed to

498 10^7 *S. boulardii* (*S. boulardii ΔURA3*) competent cells prepared on the same day. For **SpCas9**, 2μg

23

499   of Linear donor DNA and 1.5µg of gRNA plasmids were transformed to 10^7 freshly prepared

500   chemical competent *S. boulardii ΔURA3* cells containing SpCas9 plasmid. For **LbCas12a**, 2µg of

501   Linear donor DNA and 1.5µg of gRNA plasmids were transformed to 10^7 freshly prepared

502   chemical competent *S. boulardii ΔURA3* cells LbCas12a plasmid.

503

504   Overnight cultures of *S. boulardii ΔURA3* were grown in YPD only for **Homologous**

505   **Recombination,** *S. boulardii ΔURA3* containing the **SpCas9** plasmid were grown in YPD + 100

506   µg/mL nourseothricin, and *S. boulardii ΔURA3* containing the **LbCas12a** plasmid were grown in

507   YPD + 200 µg/mL G418 were subinoculated to prewarmed YPD media with or without antifungals

508   at an OD_{600} of 0.25 and incubated at 37 °C with shaking at 250 rpm until cultures reached an

509   OD_{600} of 0.9-1.0. Cultures were then centrifuged at 3000 xg for 5 min. Cells were then washed

510   twice with 0.5 and 0.1 volumes of sterile DI water at room temperature at 3000xg for 5 min. The

511   cells then were transformed according to the protocol described above, with the exception that

512   heat shocked cells were spun down, resuspended in YPD, and incubated for 3 hours at 37 °C.

513   Transformed cells were then spread on Yeast Complete Synthetic Media (CSM) without uracil

514   plates with or without antibiotics. Plates were incubated at 37 °C for 2-4 days. Integration was

515   verified with colony PCR.

516

517   **Combinatorial Pathway Assembly**

518   Prior to library assembly, promoter, gene, and terminator part plasmids were assembled into

519   'entry vector' plasmids by BsmBI assembly. These plasmids had BsaI overhangs and follow the

520   'Yeast golden gate toolkit' standard [deuber gg]. Backbones were assembled for subcloning of

24

521 the transcriptional units. These backbones housed the appropriate homology arms for later final

522 assembly of transcriptional units into a full pathway. BsaI assembly of transcriptional units into

523 the matching backbone was completed by combining 10 fmol of each promoter part plasmid (to

524 a total of 100 fmol) with 100 fmol of gene, terminator, and backbone plasmids. Reaction mixtures

525 included 0.5 μL of BsaI-HF v2, 0.5 μL of T7 DNA Ligase, and 1 μL of T4 DNA ligase buffer (NEB),

526 and underwent 50 cycles of golden gate assembly (2 minutes at 42 °C, 5 minutes at 16 °C), before

527 a single 30 minute final digestion at 60 °C, and 10 minutes of heat inactivation at 80 °C.

528 Subsequently, we have noticed that final digestion steps of 5 minutes at 42 °C are more optimal

529 for BsaI assembly[59]. Transcriptional units were amplified directly from the golden gate mixture

530 using 1 μL of reaction mixture as template in 50 μL Q5 Hot-Start Master Mix reactions (NEB). PCR

531 reactions were performed according to manufacturer's instructions and cleaned up using clean

532 and concentrate kits (D4004-Zymo Research). 600 nM of each amplified transcriptional unit

533 library was transformed using the lithium acetate protocol described above. Cells were recovered

534 for 1 hour in YPD prior to dividing the culture into 5 aliquots of 200 μL and plating on yeast

535 nitrogen base plus amino acids without uracil (Sigma).

536

537 **Pathway Sequencing.**

538 Random colonies were collected in 1.5 centrifuge tubes and resuspended in 1 ml of 10 mg/ml

539 Lysing Enzymes from *Trichoderma harzianum* (L1412 Sigma). The cells were incubated in the

540 lysing enzyme at 37 °C for 3 hours and then the ZymoPURE Plasmid Miniprep (D4208T) was used

541 to miniprep the plasmids. The Lysing Enzymes from Trichoderma harzianum help digest *S.*

542 *boulardii*'s wall and produce protoplasts that are easy to miniprep. 2μl of the miniprep product

25

543   was then used as a template to amplify the assembled region with primers complementary to

544   the pathway genes or terminators, as the ordering of these was common to all constructs. The

545   PCR product was then sent for Sanger sequencing (Genewiz, NJ,USA) to verify the promoters

546   assigned for each gene.

547

548   **Antifungal Minimum Inhibitory Concentration tests in *S. boulardii*:**

549   3 biological replicates of *S. boulardii* (ATCC-MYA796) were grown overnight in YPD media.

550   Overnight cultures were sub-inoculated into YPD media with different antifungal concentrations

551   ranging from 0 µg/ml to 200 µg/ml in a 96 well plate at starting OD_{600} 0.02 and grown for 36

552   hours in a plate reader (BioTek Synergy™ H1, Shake Mode: Double Orbital, Orbital Frequency:

553   continuous shake 365 cpm, Interval: 10 minutes). Geneticin (G418), Nourseothricin, Zeocin,

554   Hygromycin B were used in this study.

555

556   **Extraction of β-carotene from *S. boulardii* cultures.**

557   3 replicates of each β-carotene producing *S. boulardii* strain were inoculated into 1 mL CSM

558   without uracil (2.5% glucose) and and grown overnight in a shaking incubator at 250 rpm at 37 °C.

559   Overnight cultures were then subinoculated (1:100) into 30 mL CSM without uracil (2.5% glucose)

560   and grown for 3 days in a rotary incubator at 250 rpm at 37 °C. After 3 days, $2*10^9$ cells were

561   collected by centrifuging at 4 °C at 5000g for 5 minutes. The media was discarded and the cells

562   were washed with 10 mL water and were centrifuged at 4 °C at 5000g for another 5 minutes.

563   After the water was discarded, the cells were resuspended in 500 µL water and transferred into

564   ZR Bashing Bead Tubes (Zymo Research, CA). The ZR Bashing tubes were centrifuged for 1 minute

26

565   at 8000g to discard the water. 500 μL acetone was then added into the bashing tubes. The tubes

566   containing the cells, acetone, and lysis beads then transferred to a homogenizer (TissueLyser,

567   Qiagen, Germany) for physical lysis (Lysis duration: 10 minutes, frequency: 30/s). The cells and

568   the lysates then centrifuged at 16000g for 5 minutes at 4 °C. The supernatants (acetone lysate)

569   were transferred to 1.5 mL black microcentrifuge tubes. Fresh acetone was then added to the

570   bashing tubes, and lysis steps were repeated 2 more times, at which point the cell pellets were

571   completely white. β-carotene extracts were dried by speed vac (aqueous solvent, 30 °C for 2

572   hours). Dried β-carotene pellets were reconstituted in 500 μL acetone and stored at -20 °C in the

573   dark.

574

Detection of β-carotene by HPLC.

575

576   5μL of each sample was processed in an Agilent 1260 Infinity high performance liquid-

577   chromatography (HPLC) system (Agilent Technologies, CA, USA). 0.002 mM naphthalene solution

578   was used as internal control and pure β-carotene (Thermo Fisher, Waltham, MA) at varying

579   concentrations (mg/mL) 0.00625, 0.0125, 0.025, 0.05, 0.0625, 0.125, 0.25, 0.5, 0.625, 1.25, 2.5,

580   5) as external control. The channels used for internal control and β-carotene detection were 275

581   nm and 453 nm, respectively. The column used in the system was an Agilent HC-C28 Reversed

582   Phase column (4.6 x 250 mm, 50 μL) (Agilent Technologies, CA, USA). The composition of the

583   mobile phase was acetonitrile:methanol:isopropanol (v/v/v: 85/10/5) The flow rate for the

584   mobile phase was 3 mL/min.

585

References

586

587   1.   Tiago, F. C. P. *et al.* Adhesion to the yeast cell surface as a mechanism for trapping

588   pathogenic bacteria by Saccharomyces probiotics. *J. Med. Microbiol.* **61**, 1194–1207 (2012).

589   2.   Khatri, I., Tomar, R., Ganesan, K., Prasad, G. S. & Subramanian, S. Complete genome

590   sequence and comparative genomics of the probiotic yeast Saccharomyces boulardii. *Sci.*

591   *Rep.* **7**, 371 (2017).

592   3.   O'Toole, P. W., Marchesi, J. R. & Hill, C. Next-generation probiotics: the spectrum from

593   probiotics to live biotherapeutics. *Nat Microbiol* **2**, 17057 (2017).

594   4.   Mimee, M., Citorik, R. J. & Lu, T. K. Microbiome therapeutics - Advances and challenges.

595   *Adv. Drug Deliv. Rev.* **105**, 44–54 (2016).

596   5.   Pedrolli, D. B. *et al.* Engineering Microbial Living Therapeutics: The Synthetic Biology

597   Toolbox. *Trends Biotechnol.* **37**, 100–115 (2019).

598   6.   Ozdemir, T., Fedorec, A. J. H., Danino, T. & Barnes, C. P. Synthetic Biology and Engineered

599   Live Biotherapeutics: Toward Increasing System Complexity. *Cell Syst* **7**, 5–16 (2018).

600   7.   Ferreiro, A., Crook, N., Gasparrini, A. J. & Dantas, G. Multiscale Evolutionary Dynamics of

601   Host-Associated Microbiomes. *Cell* **172**, 1216–1227 (2018).

602   8.   Bourdeau, R. W. *et al.* Acoustic reporter genes for noninvasive imaging of microorganisms

603   in mammalian hosts. *Nature* **553**, 86–90 (2018).

604   9.   Riglar, D. T. *et al.* Engineered bacteria can function in the mammalian gut long-term as live

605   diagnostics of inflammation. *Nat. Biotechnol.* **35**, 653–658 (2017).

606   10. Kotula, J. W. *et al.* Programmable bacteria detect and record an environmental signal in the

607   mammalian gut. *Proc. Natl. Acad. Sci. U. S. A.* **111**, 4838–4843 (2014).

608   11. Shaw, W. M. *et al.* Engineering a Model Cell for Rational Tuning of GPCR Signaling. *Cell* **177**,

609   782–796.e27 (2019).

610   12. Rugbjerg, P. & Sommer, M. O. A. Overcoming genetic heterogeneity in industrial

611   fermentations. *Nat. Biotechnol.* (2019) doi:10.1038/s41587-019-0171-6.

612   13. Almeida, A. *et al.* A new genomic blueprint of the human gut microbiota. *Nature* **568**, 499–

613   504 (2019).

614   14. Sender, R., Fuchs, S. & Milo, R. Revised Estimates for the Number of Human and Bacteria

615   Cells in the Body. *PLoS Biol.* **14**, e1002533 (2016).

616   15. Crook, N. *et al.* Adaptive Strategies of the Candidate Probiotic E. coli Nissle in the

617   Mammalian Gut. *Cell Host Microbe* **25**, 499–512.e8 (2019).

618   16. Isabella, V. M. *et al.* Development of a synthetic live bacterial therapeutic for the human

619   metabolic disease phenylketonuria. *Nat. Biotechnol.* **36**, 857–864 (2018).

620   17. Kurtz, C. B. *et al.* An engineered E. coli Nissle improves hyperammonemia and survival in

621   mice and shows dose-dependent exposure in healthy humans. *Sci. Transl. Med.* **11**, (2019).

622   18. Ho, C. L. *et al.* Engineered commensal microbes for diet-mediated colorectal-cancer

623   chemoprevention. *Nat Biomed Eng* **2**, 27–37 (2018).

624   19. Hwang, I. Y. *et al.* Engineered probiotic Escherichia coli can eliminate and prevent

625   Pseudomonas aeruginosa gut infection in animal models. *Nat. Commun.* **8**, 15028 (2017).

626   20. Langdon, A., Crook, N. & Dantas, G. The effects of antibiotics on the microbiome

627   throughout development and alternative approaches for therapeutic modulation. *Genome*

628   *Med.* **8**, 39 (2016).

629   21. Sweere, J. M. *et al.* Bacteriophage trigger antiviral immunity and prevent clearance of

630   bacterial infection. *Science* **363**, (2019).

631   22. Brunk, E. *et al.* Characterizing posttranslational modifications in prokaryotic metabolism

632   using a multiscale workflow. *Proc. Natl. Acad. Sci. U. S. A.* **115**, 11096–11101 (2018).

633   23. Jiang, T. T. *et al.* Commensal Fungi Recapitulate the Protective Benefits of Intestinal

634   Bacteria. *Cell Host Microbe* **22**, 809–816.e4 (2017).

635   24. Huseyin, C. E., O'Toole, P. W., Cotter, P. D. & Scanlan, P. D. Forgotten fungi-the gut

636   mycobiome in human health and disease. *FEMS Microbiol. Rev.* **41**, 479–511 (2017).

637   25. Wheeler, M. L. *et al.* Immunological Consequences of Intestinal Fungal Dysbiosis. *Cell Host

638   Microbe* **19**, 865–873 (2016).

639   26. Hamad, I. *et al.* Culturomics and Amplicon-based Metagenomic Approaches for the Study

640   of Fungal Population in Human Gut Microbiota. *Sci. Rep.* **7**, 16788 (2017).

641   27. Richard, M. L. & Sokol, H. The gut mycobiota: insights into analysis, environmental

642   interactions and role in gastrointestinal diseases. *Nat. Rev. Gastroenterol. Hepatol.* **16**,

643   331–345 (2019).

644   28. Shao, T.-Y. *et al.* Commensal Candida albicans Positively Calibrates Systemic Th17

645   Immunological Responses. *Cell Host Microbe* **25**, 404–417.e6 (2019).

646   29. Tso, G. H. W. *et al.* Experimental evolution of a fungal pathogen into a gut symbiont.

647   *Science* **362**, 589–595 (2018).

648   30. Hotel, A. C. P. & Cordoba, A. Health and nutritional properties of probiotics in food

649   including powder milk with live lactic acid bacteria. *Prevention* **5**, 1–10 (2001).

650   31. van der Aa Kühle, A. & Jespersen, L. The taxonomic position of Saccharomyces boulardii as

651   evaluated by sequence analysis of the D1/D2 domain of 26S rDNA, the ITS1-5.8S rDNA-ITS2

652   region and the mitochondrial cytochrome-c oxidase II gene. *Syst. Appl. Microbiol.* **26**, 564–

653   571 (2003).

654   32. Hudson, L. E. *et al.* Characterization of the Probiotic Yeast Saccharomyces boulardii in the

655   Healthy Mucosal Immune System. *PLoS One* **11**, e0153351 (2016).

656   33. Liu, J.-J. *et al.* Metabolic Engineering of Probiotic Saccharomyces boulardii. *Appl. Environ.*

657   *Microbiol.* **82**, 2280–2287 (2016).

658   34. Fietto, J. L. R. *et al.* Molecular and physiological comparisons between Saccharomyces

659   cerevisiae and Saccharomyces boulardii. *Can. J. Microbiol.* **50**, 615–621 (2004).

660   35. Rodrigues, A. C. P. *et al.* Saccharomyces boulardii stimulates sIgA production and the

661   phagocytic system of gnotobiotic mice : immunomodulation by probiotic. *J. Appl.*

662   *Microbiol.* **89**, 404–414 (2000).

663   36. Palma, M. L., Garcia-Bates, T. M., Martins, F. S. & Douradinha, B. Genetically engineered

664   probiotic Saccharomyces cerevisiae strains mature human dendritic cells and stimulate

665   Gag-specific memory CD8+ T cells ex vivo. *Appl. Microbiol. Biotechnol.* **103**, 5183–5192

666   (2019).

667   37. Michael, S. *et al.* Quantitative phenotyping of inflammatory bowel disease in the IL-10-

668   deficient mouse by use of noninvasive magnetic resonance imaging. *Inflamm. Bowel Dis.*

669   **19**, 185–193 (2013).

670   38. Lee, M. E., DeLoache, W. C., Cervantes, B. & Dueber, J. E. A Highly Characterized Yeast

671   Toolkit for Modular, Multipart Assembly. *ACS Synth. Biol.* **4**, 975–986 (2015).

672   39. Karim, A. S., Curran, K. A. & Alper, H. S. Characterization of plasmid burden and copy

673   number in Saccharomyces cerevisiae for optimization of metabolic engineering

674   applications. *FEMS Yeast Res.* **13**, 107–116 (2013).

675   40. Ghim, C.-M., Lee, S. K., Takayama, S. & Mitchell, R. J. The art of reporter proteins in science:

676   past, present and future applications. *BMB Rep.* **43**, 451–460 (2010).

677   41. Xiao, Y., Bowen, C. H., Liu, D. & Zhang, F. Exploiting nongenetic cell-to-cell variation for

678   enhanced biosynthesis. *Nat. Chem. Biol.* **12**, 339–344 (2016).

679   42. Mundt, M., Anders, A., Murray, S. M. & Sourjik, V. A System for Gene Expression Noise

680   Control in Yeast. *ACS Synth. Biol.* **7**, 2618–2626 (2018).

681   43. Yuan, T. *et al.* Construction, characterization and application of a genome-wide promoter

682   library in Saccharomyces cerevisiae. *Frontiers of Chemical Science and Engineering* **11**, 107–

683   116 (2017).

684   44. Partow, S., Siewers, V., Bjørn, S., Nielsen, J. & Maury, J. Characterization of different

685   promoters for designing a new expression vector in Saccharomyces cerevisiae. *Yeast* **27**,

686   955–964 (2010).

687   45. Datta, S., Annapure, U. S. & Timson, D. J. Different specificities of two aldehyde

688   dehydrogenases from Saccharomyces cerevisiae var. boulardii. *Biosci. Rep.* **37**, (2017).

689   46. Curran, K. A., Karim, A. S., Gupta, A. & Alper, H. S. Use of expression-enhancing terminators

690   in Saccharomyces cerevisiae to increase mRNA half-life and improve gene expression

691   control for metabolic engineering applications. *Metab. Eng.* **19**, 88–97 (2013).

692   47. Wei, L., Wang, Z., Zhang, G. & Ye, B. Characterization of Terminators in Saccharomyces

693   cerevisiae and an Exploration of Factors Affecting Their Strength. *Chembiochem* **18**, 2422–

694   2427 (2017).

695   48. Yamanishi, M. *et al.* A genome-wide activity assessment of terminator regions in

696   Saccharomyces cerevisiae provides a "terminatome" toolbox. *ACS Synth. Biol.* **2**, 337–347

697   (2013).

698   49. Struhl, K. & Segal, E. Determinants of nucleosome positioning. *Nat. Struct. Mol. Biol.* **20**,

699   267–273 (2013).

700   50. Raschmanová, H., Weninger, A., Glieder, A., Kovar, K. & Vogl, T. Implementing CRISPR-Cas

701   technologies in conventional and non-conventional yeasts: Current state and future

702   prospects. *Biotechnol. Adv.* **36**, 641–665 (2018).

703   51. Yuan, J. & Ching, C. B. Combinatorial assembly of large biochemical pathways into yeast

704   chromosomes for improved production of value-added compounds. *ACS Synth. Biol.* **4**, 23–

705   31 (2015).

706   52. Lee, M. E., Aswani, A., Han, A. S., Tomlin, C. J. & Dueber, J. E. Expression-level optimization

707   of a multi-enzyme pathway in the absence of a high-throughput assay. *Nucleic Acids Res.*

708   **41**, 10668–10678 (2013).

709   53. Wingler, L. M. & Cornish, V. W. Reiterative Recombination for the in vivo assembly of

710   libraries of multigene pathways. *Proc. Natl. Acad. Sci. U. S. A.* **108**, 15135–15140 (2011).

711   54. Verwaal, R. *et al.* High-level production of beta-carotene in Saccharomyces cerevisiae by

712   successive transformation with carotenogenic genes from Xanthophyllomyces

713   dendrorhous. *Appl. Environ. Microbiol.* **73**, 4342–4350 (2007).

714   55. Cunningham, F. X. & Gantt, E. One ring or two? Determination of ring number in

715   carotenoids by lycopene ε-cyclases. *Proc. Natl. Acad. Sci. U. S. A.* **98**, 2905–2910 (2001).

716   56. Naseri, G., Behrend, J., Rieper, L. & Mueller-Roeber, B. COMPASS for rapid combinatorial

717   optimization of biochemical pathways based on artificial transcription factors. *Nat.*

718   *Commun.* **10**, 2615 (2019).

719   57. Kennedy, E. A., King, K. Y. & Baldridge, M. T. Mouse Microbiota Models: Comparing Germ-

720   Free Mice and Antibiotics Treatment as Tools for Modifying Gut Bacteria. *Front. Physiol.* **9**,

721   1534 (2018).

722   58. Barc, M.-C. *et al.* Molecular analysis of the digestive microbiota in a gnotobiotic mouse

723   model during antibiotic treatment: Influence of Saccharomyces boulardii. *Anaerobe* **14**,

724   229–233 (2008).

725   59. Potapov, V. *et al.* Comprehensive Profiling of Four Base Overhang Ligation Fidelity by T4

726   DNA Ligase and Application to DNA Assembly. *ACS Synth. Biol.* **7**, 2665–2674 (2018).

727   60. Gietz, R. D., Daniel Gietz, R. & Schiestl, R. H. High-efficiency yeast transformation using the

728   LiAc/SS carrier DNA/PEG method. *Nature Protocols* vol. 2 31–34 (2007).

729   61. Gietz, R. D., Daniel Gietz, R. & Schiestl, R. H. Quick and easy yeast transformation using the

730   LiAc/SS carrier DNA/PEG method. *Nature Protocols* vol. 2 35–37 (2007).
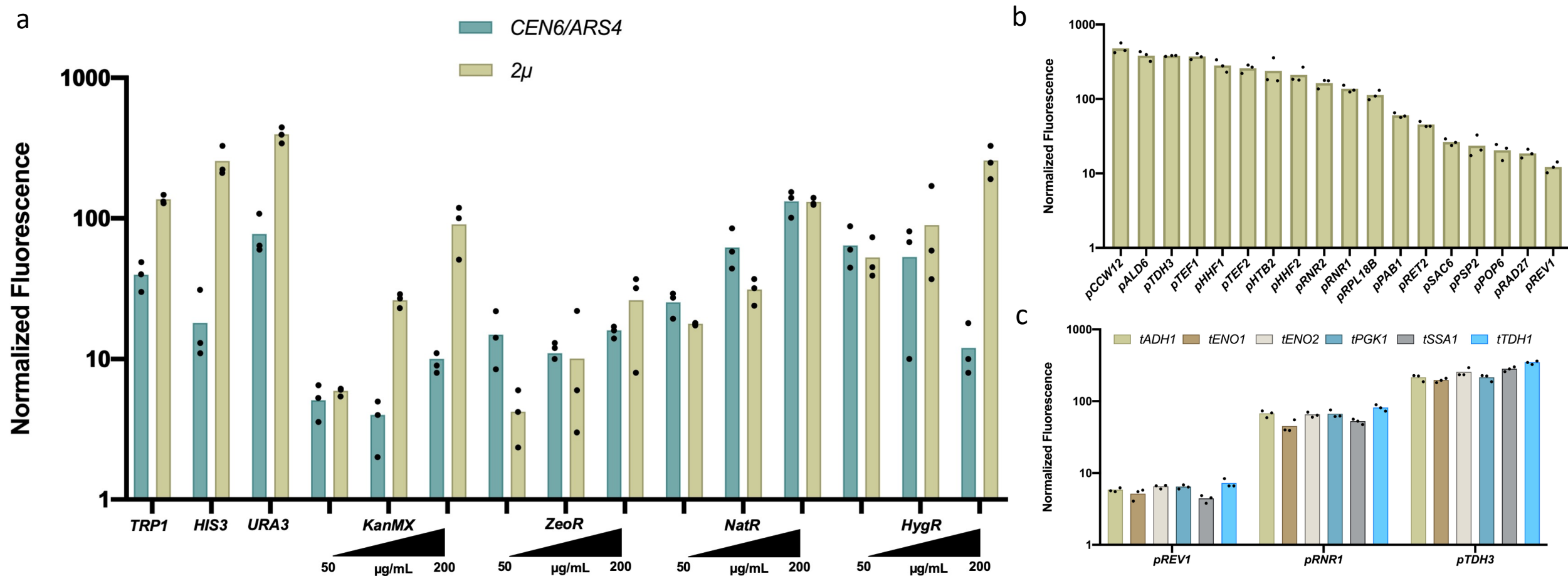
Figure 1. Characterization of *S. boulardii* (a) markers and origins of replication, (b) promoters, and (c) terminators *in vitro*. a) 3 auxotrophic (*URA3, HIS3, TRP1*) and 4 antifungal (*KanMX, ZeoR, NatR, HygR*) markers were cloned in plasmids containing the *TDH3* promoter, mRuby2 fluorescent protein and *TDH1* terminator. Centromeric (*CEN6/ARS4*) and episomal (*2µ*) origins were cloned in combination with the 7 selective markers. Plasmids with antifungal markers were tested in 3 different antifungal concentrations (50, 100 and 200 µg/mL). **b)** 18 constitutive promoters were cloned 5' of the *mRuby2* fluorescent protein and the *TDH1* terminator. **c)** 5 terminators were cloned 3' of 3 different promoters at different strength (*pTDH3*-strong, *pRNR1*-medium and *pREV1*-weak) and the *mRuby2* fluorescent protein. Absolute fluorescence values were obtained via flow cytometry for 3 biological replicates (n=3). Absolute fluorescence values were normalized to fluorescent values of cells harboring the spacer plasmid. The height of the bars represents the normalized mean fluorescent value of 3 biological replicates and the black dots show the normalized mean of each biological replicate.
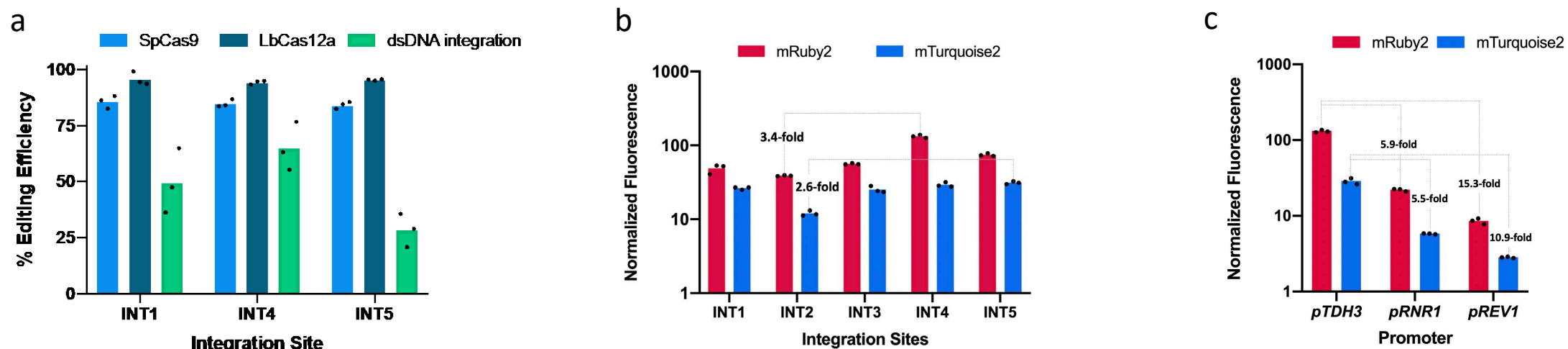
Figure 2. *S. boulardii* **genomic location impacts gene expression, and comparison of genome editing techniques. a.** Editing efficiency at 3 different loci using 3 different methods: CRISPR/SpCas9 (SpCas9), CRISPR/LbCas12a (LbCas12a) and un-assisted linear dsDNA integration (dsDNA integration). 3 different guides were used for both SpCas9 and LbCas12a for each site. Each dot represents one guide. 3 replicate cultures were transformed with the DNA repair template to measure the efficiency of genome editing in *Sb* via dsDNA integration. Table S1 shows the number of colonies screen for each method. **b.** Effect of chromosomal locus on the expression of the fluorescent genes mRuby2 and mTurqouise2. The dotted lines show the fold change between the expression of mRuby2 and mTurquoise2 between the highest and lowest expression among all the integration sites. Each dot represents one biological replicate. **c.** The effects of promoter (strong, medium, or weak) on gene expression at the same chromosomal locus. The dotted lines show the fold change between the expression of *mRuby2* and mTurquoise2 using different promoters. Each dot represents one biological replicate.
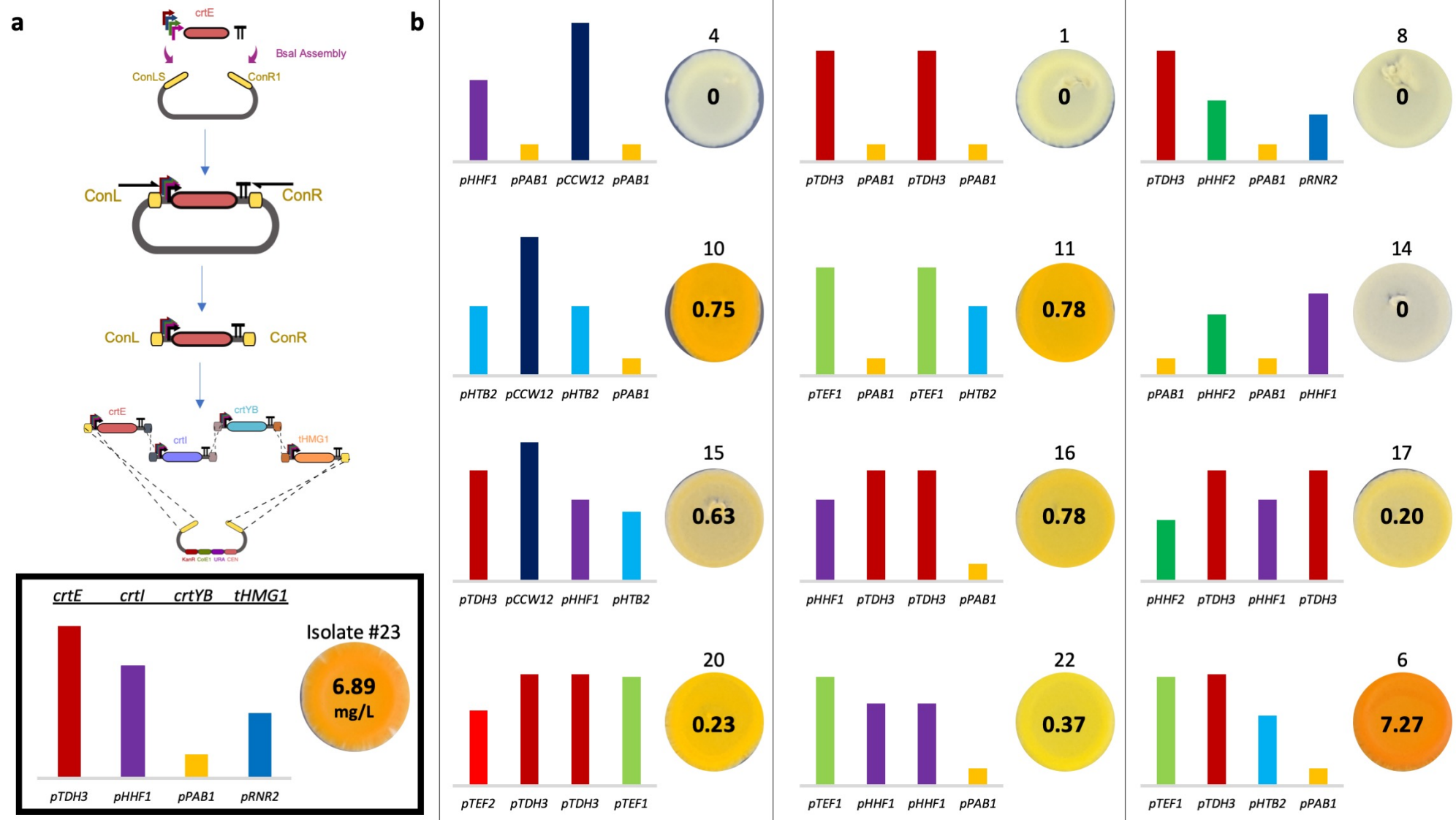
Figure 3. Combinatorial Assembly of the β-carotene Pathway in *Saccharomyces boulardii*. a) Overview of assembly steps. Genes in the β-carotene pathway were randomly cloned behind 9 promoters (*pTDH3, pCCW12, pHHF2, pTEF1, pTEF2, pHHF1, pHTB2, pPAB1, pRNR2*). tSSA1, tADH1, tTDH1 and tENO1 terminators were cloned behind *crtE, crtI, crttYB-2* and *tHMG1*, respectively. The backbone plasmid contains Type1 and Type2 YTK connectors to enable in vivo *S. boulardii* assembly. Promoter-gene-terminator regions between the two connectors were amplified and the PCR products were transformed in *S. boulardii* for pathway assembly into a linear backbone via connector-assisted homologous recombination, as described in the Methods Section. **b)** Sequencing and β-carotene quantification results of isolates from yeast transformation plates (Supplementary Figure S8b). 13 out of 28 isolates (Supplementary Figure S8d) were selected to proceed with sequencing and β-carotene production quantification based on stability of colony color after 3 serial passages. Promoter sequences were confirmed by Sanger sequencing with reverse primer binding on the gene of interest (backbone for *tHMG1*) and forward primer binding on the terminator of the previous gene (backbone for *crtE*). Quantification of β-carotene was done by high-performance liquid chromatography (HPLC) as described in the Methods section. The spot images were taken from Supplementary Figure S8d. Number above the spots corresponds to the spot number on isolate plate on Supplementary Figure S8d. The bar heights represent the normalized fluorescence values in linear scale for each promoter according to promoter characterization work (Figure 1a). The numbers in the center of the spots corresponds to average of β-carotene produced by 3 biological replicate of each isolate in one liter of saturated yeast culture.
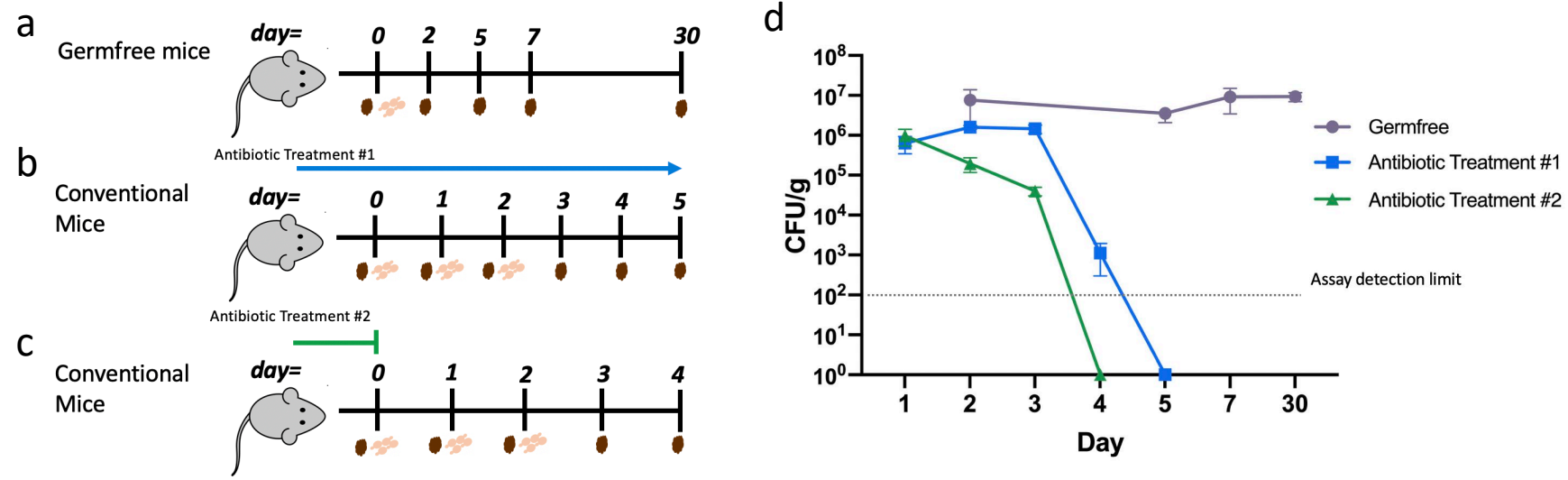
Figure 4. Microbial competition reduces *S. boulardii* residence time in mice. **a.** Germfree mouse model gavaged with *S. boulardii* on day 0. **b** Conventional mouse model treated with 1mg/ml penicillin and 2mg/ml streptomycin in the drinking water for 4 days prior to 3 *S.b::NatR* treatments every 24 hours (antibiotics were replenished every 4 days.) **c**. Conventional mouse model treated with 1mg/ml penicillin and 2mg/ml streptomycin in the drinking water for 4 days prior to 3 *S.b::NatR* treatments every 24 hours (antibiotic treatment was stopped on day 0.) **d.** Fecal carriage of *S.b* in the three mice models. Fecal samples were collected as shown in the timelines and plated on YPD media for the gnotobiotic model and YPD containing antibiotics for the conventional mice models. The dashed line shows the detection limit of our assay. Error bars indicate the standard deviation observed among 4 germ free mice, 3 conventional mice treated with antibiotic treatment #1, and 3 conventional mice treated with antibiotic treatment #2. In all mouse models, feces were collected prior to Sb gavage during days when both occurred.
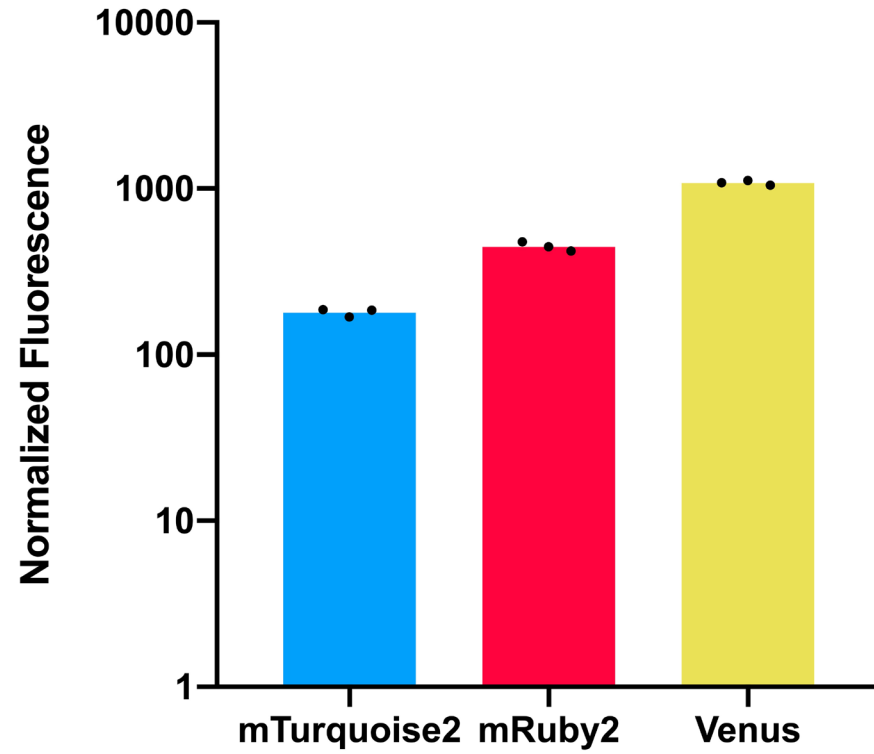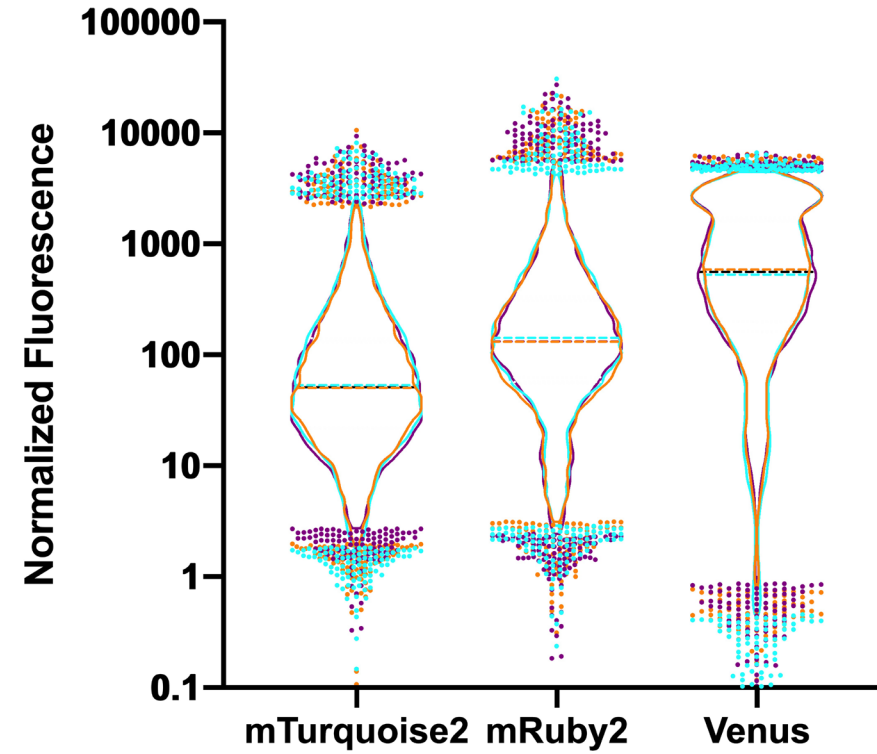
Figure S1. Characterization of Fluorescent Genes. a) 3 fluorescent genes (*mTurquoise2, mRuby2* and *Venus*) were cloned behind *TDH3* promoter and in front of *TDH1* terminator. The height of the bars represent the mean fluorescent value of 3 biological replicates (n=3). The black dots show the normalized mean of each biological replicate. **b)** Violin plots of flow cytometry data for 3 fluorescent proteins. Cyan, orange and purple represent first, second and third biological replicates, respectively. The dots represent the highest and lowest 2 percent of the cell population. Each flow cytometry run consists of 10000 events.
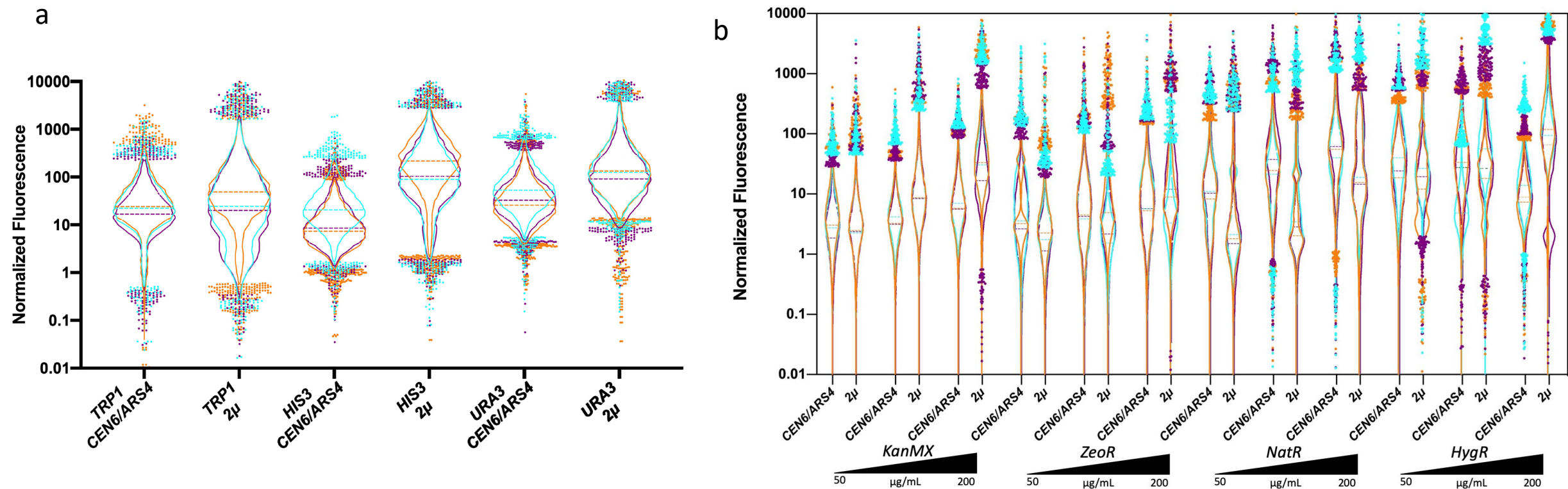
Figure S2 Characterization of selective markers and origins of replication. a) Violin plots of flow cytometry data for 3 auxotrophic markers and 2 origins of replication.
b) Violin plots of flowcytometry data for 7 antifungal markers and 2 origins of replication tested in 3 different antifungal concentrations (50, 100, 200 μg/mL).
3 auxotrophic markers, 4 antifungal markers and 2 origins of replications were cloned behind *TDH3* promoter, mRuby2 fluorescent protein and *TDH1* terminator. Cyan, orange and purple represent first, second and third biological replicates, respectively. The dots represent the highest and lowest 2 percent of the cell population. Each flow cytometry run consists of 5000-10000 events.
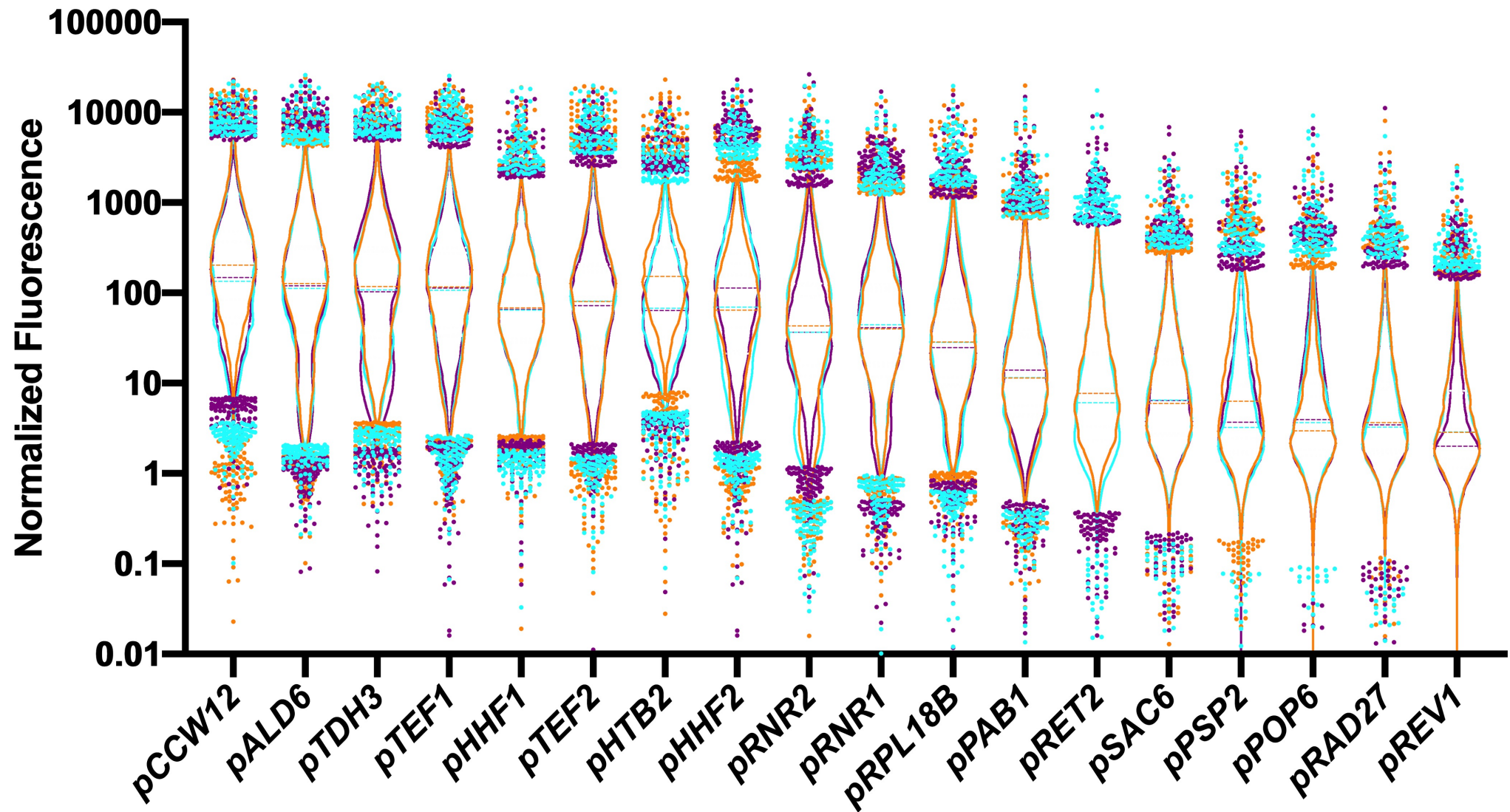
Figure S3 Characterization of Promoters. Violin plots of flowcytometry data for 18 constitutive promoters. 18 constitutive promoters were cloned in front of mRuby2 fluorescent protein and *tTDH1* terminator.
Cyan, orange and purple represent first, second and third biological replicates, respectively. The dots represent the %2 percent of the cell population. Each flowcytometry run consists of 10000 events.
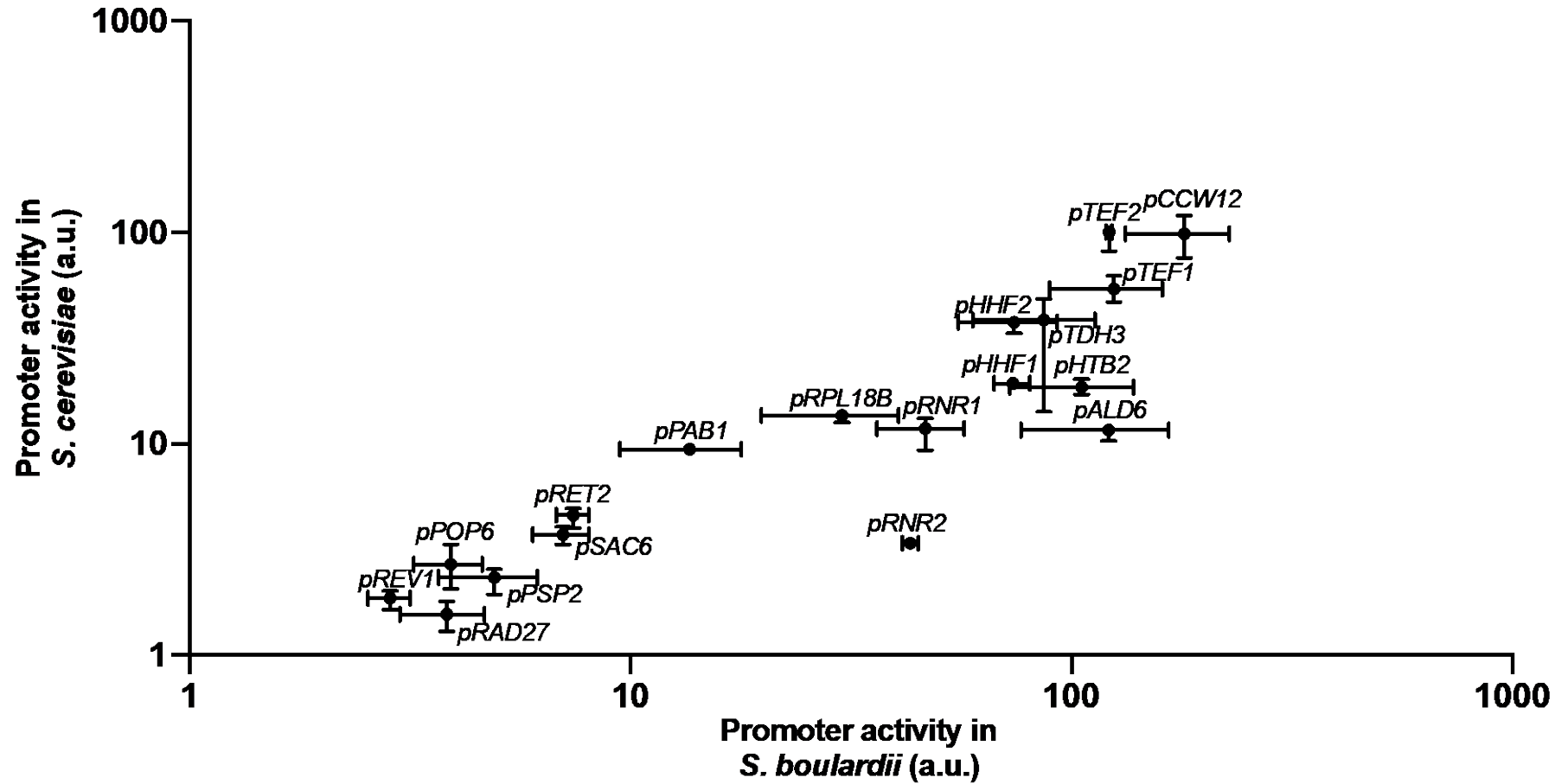
Figure S4 Comparison of constitutive promoter activity between *S. cerevisiae* and *S. boulardii*. Promoter activity of 18 constitutive promoters in *S. boulardii* (x-axis) and *S. cerevisiae* (y-axis) were plotted (R=0.81). In each synthetic construct, one constitutive promoter was cloned upstream of *mRuby2* gene. Activity of each promoter in both yeast species was determined by reading median fluorescence values produced by mRuby2 protein via flowcytometry. Dots correspond to the average median of 3 (*S. boulardii*) and 4 (*S. cerevisiae*) biological replicates and the bars correspond to maximum and minimum median value obtained by the replicates.
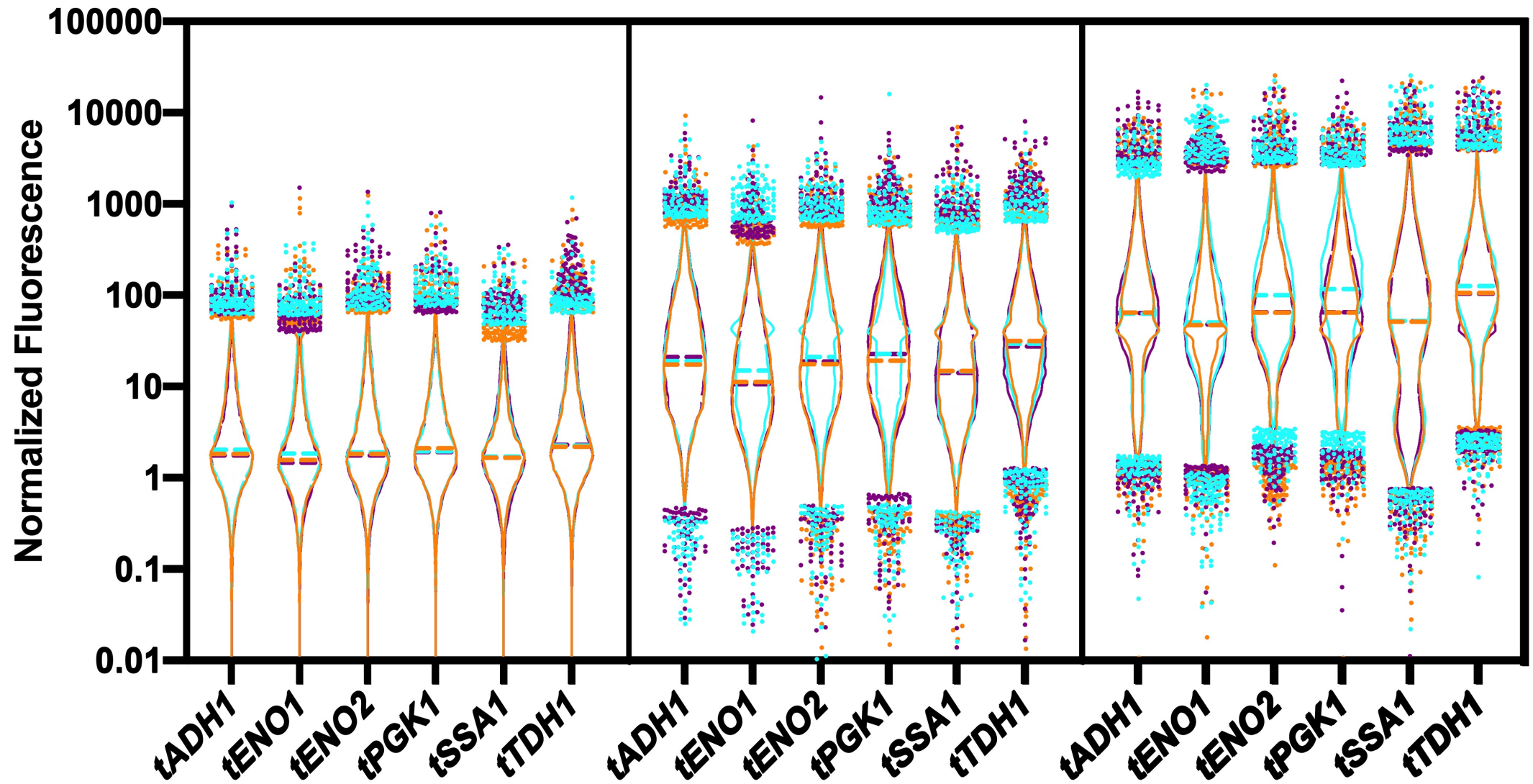
Figure S5 Characterization of Terminators. Violin plots of flowcytometry data for 5 terminators combined with 3 promoters. 5 terminators were cloned behind 3 promoters with different strength (*pTDH3*-strong-most right panel, *pRNR1*-medium-middle panel, *pREV1*-weak-most left panel) and mRuby2 fluorescent protein.

Cyan, orange and purple represent first, second and third biological replicates, respectively. The dots represent the %2 percent of the cell population. Each flowcytometry run consists of 10000 events.
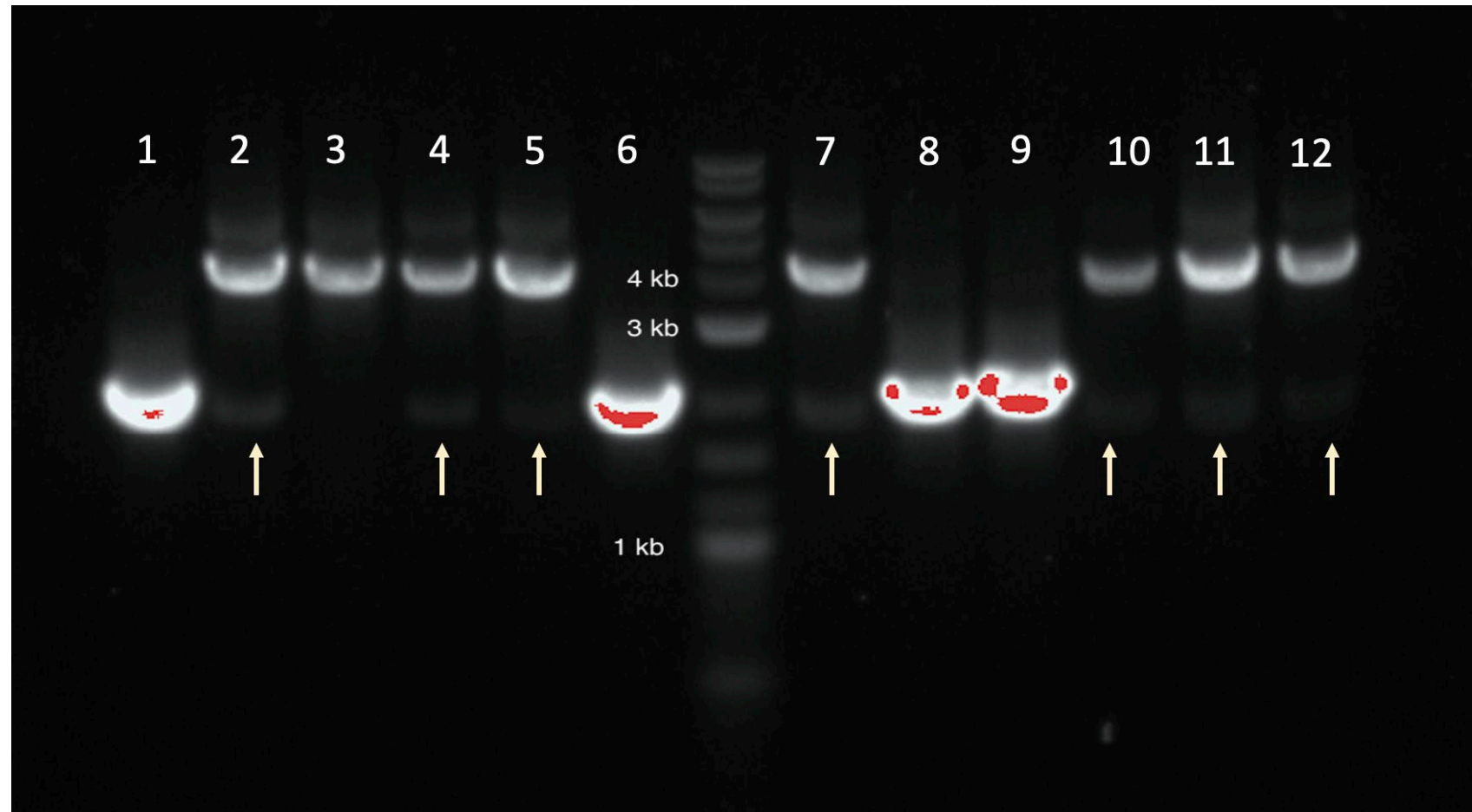
Figure S6. Colony PCR of *S. boulardii* genome editing using only homologous recombination. The gel image shows that when only donor DNA is transformed into *S. boulardii*, the cells keeps a copy of the original chromosomal locus sequence. Lanes 1-6 lanes show a PCR for correct integration into INT1. Lanes 7-12 show a PCR for correct integration into INT4. In both cases, a correct integration will yield a PCR product of 3.8 kb, while the native sequence yields a PCR product of 2.0 kb.
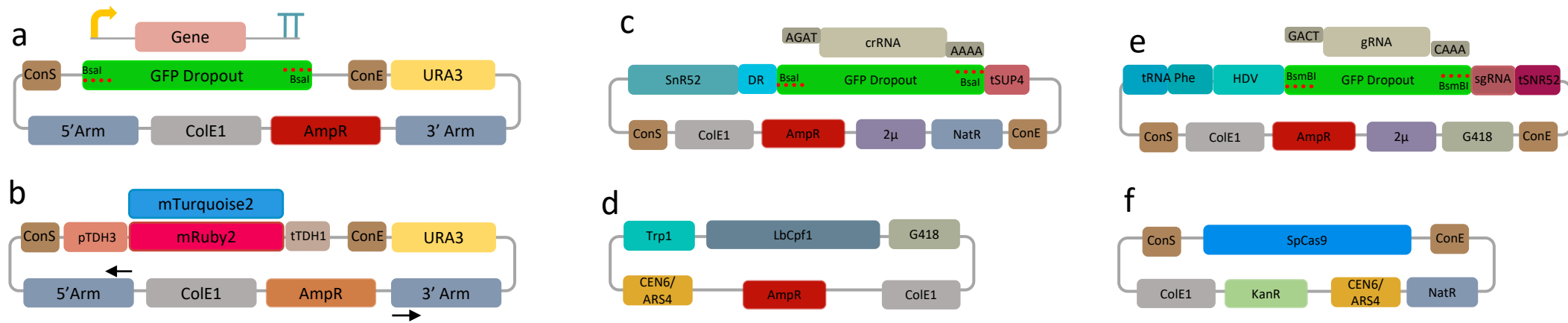
Figure S7. Genome editing plasmids. a. Vector for assembling the promoter, gene and terminator of interest. **b.** Example of constructed integration plasmid using cloning vector from a. **c.** Cloning vector with GFP dropout for constructing the CRISPR/LbCas12a crRNA **d.** CRISPR/LbCas12a expression vector. **e.** Cloning vector with GFP dropout for constructing the CRISPR/SpCas9 gRNA. **f.** CRISPR/SpCas9 expression vector. All GFP dropout vectors vectors are used in Golden Gate reactions with either BsaI or BsmBI enzymes.
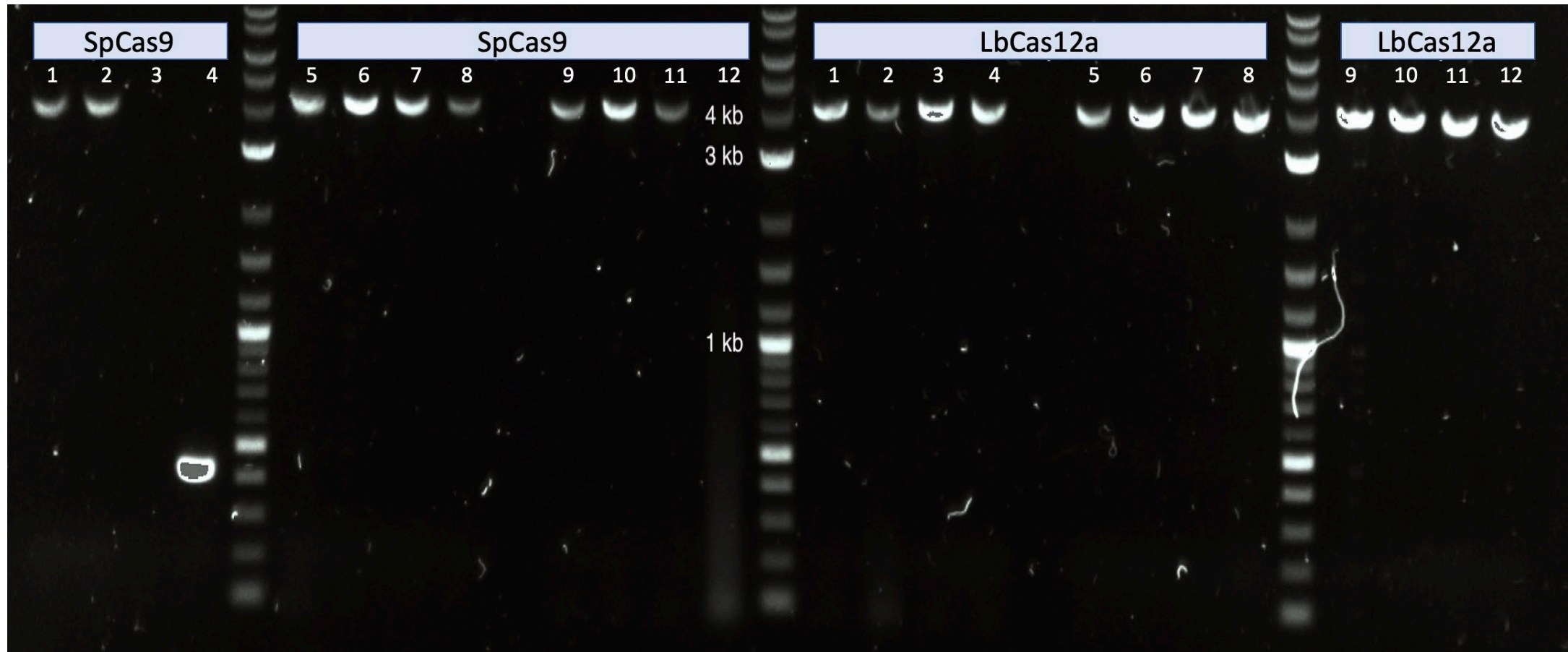
Figure S8. Colony PCR of *S. boulardii* genome editing using CRISPR/SpCas9 and CRISPR/LbCas12a. SpCas9 lanes 1-4 show a PCR screen for integration into INT1 (line 3 is failed PCR reaction and line 4 is unedited site), SpCas9 lanes 5-8 show a PCR screen for integration into INT4, and SpCas9 lanes 9-12 show a PCR screen for integration into INT5. LbCas12a lanes 1-4 show a PCR screen for integration into INT1, LbCas12a lanes 5-8 show a PCR screen for integration into INT4 and LbCas12a lanes 9-12 show a PCR screen for integration into INT5.
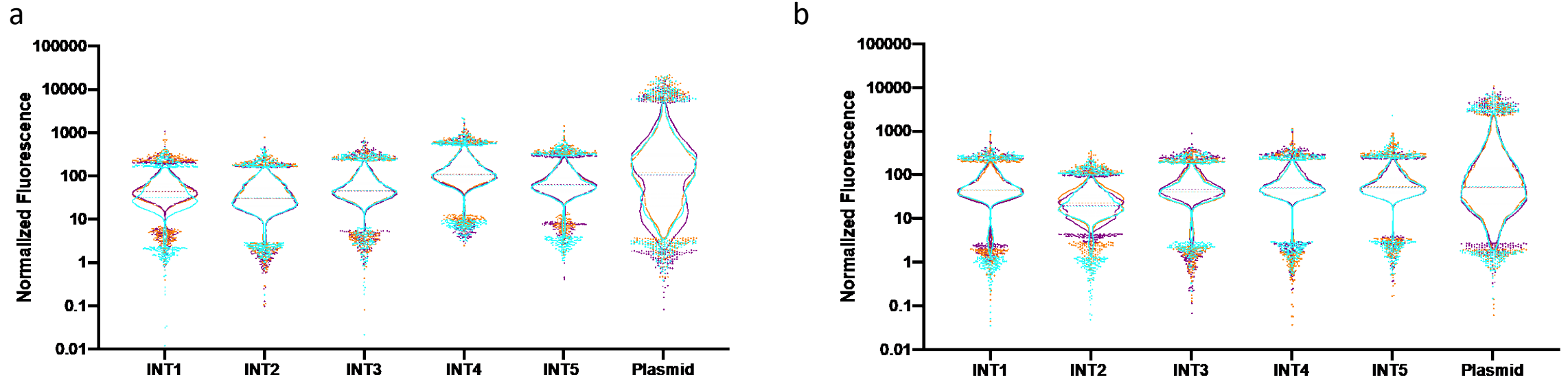
Figure S9 Effect of chromosomal locus on the expression of the fluorescent genes *mRuby2* and *mTurqouise2*. . Violin plots of flowcytometry data for **a.** *mRuby2* expression in 5 different loci in the genome compared to the expression of the same construct in plasmid with *2μ.* b. *mTurqiouse2* expression in 5 different loci in the genome compared to the expression of the same construct in plasmid with *2μ* origin. constitutive promoters.
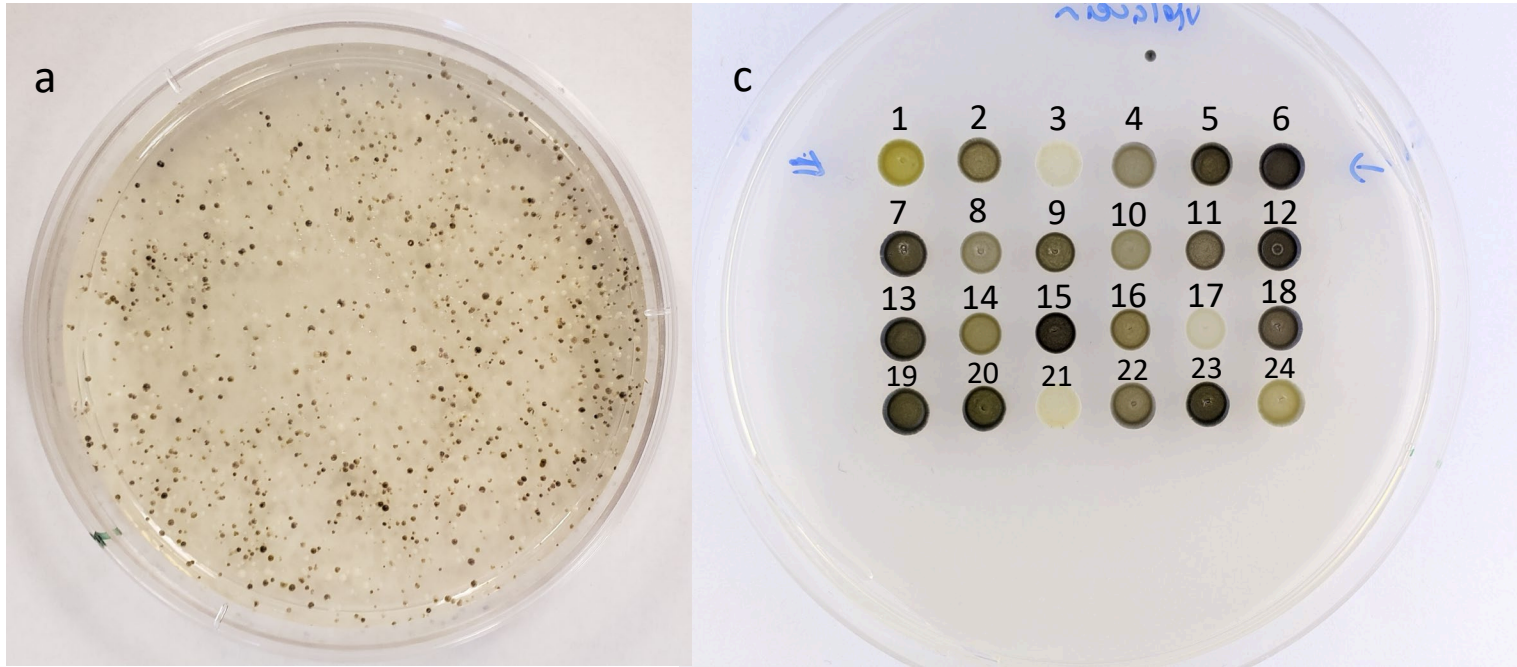
Figure S10. *in vivo* **Combinatorial Pathway Assembly in *S. boulardii*. a&b)** *S. boulardii* Transformation plates for violacein (a) and β-carotene (b) pathways. Violacein **(c)** and β-carotene (d) isolates picked from plates a &b.
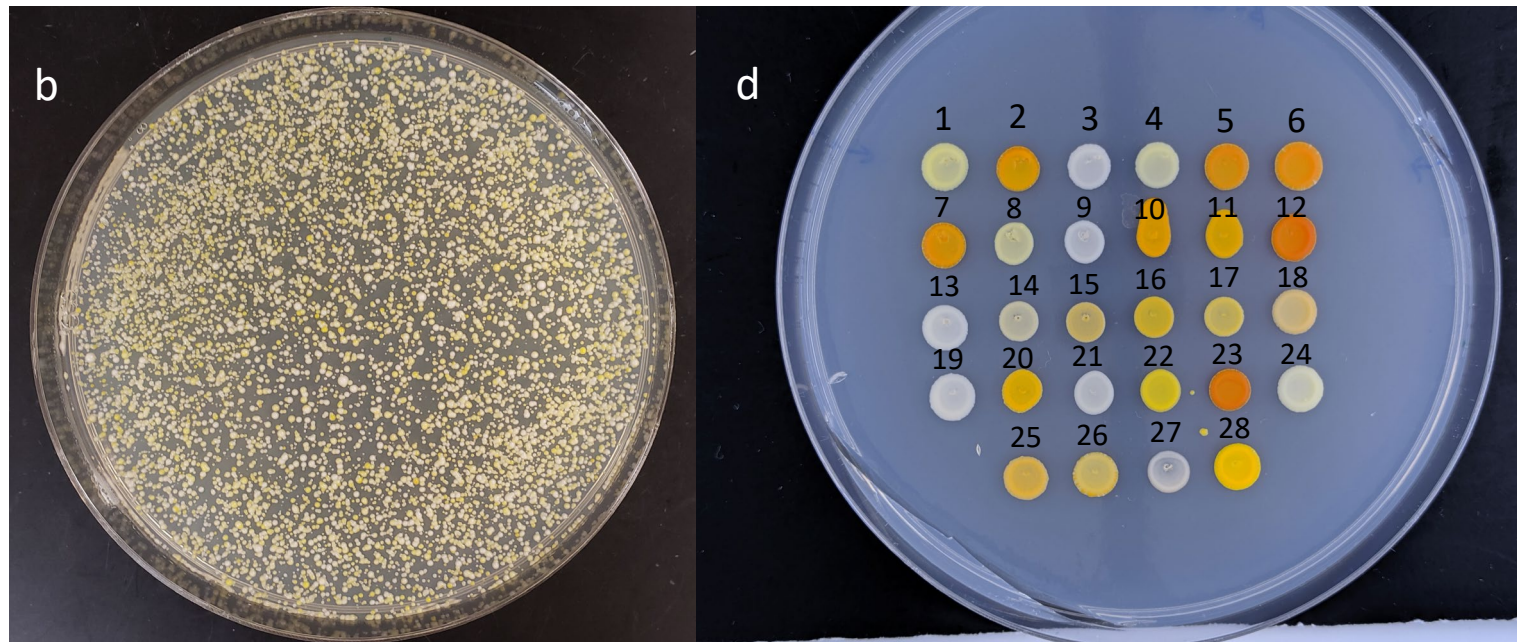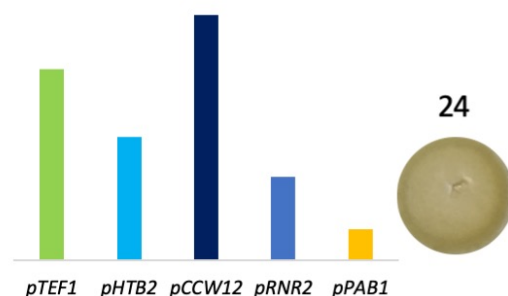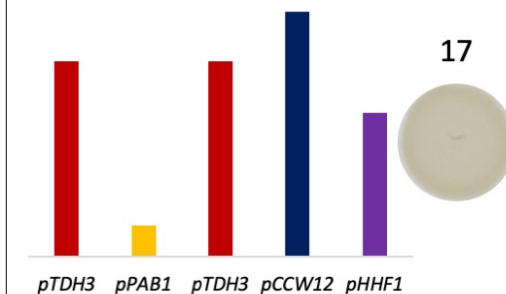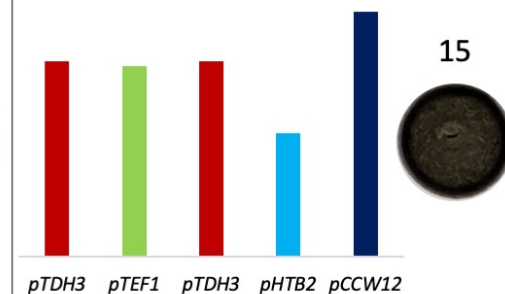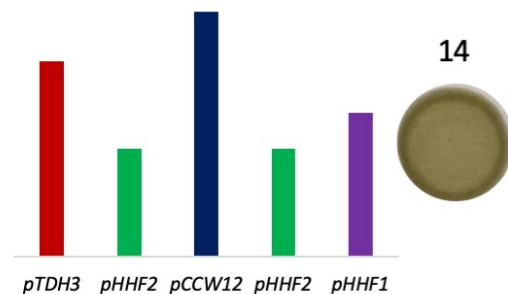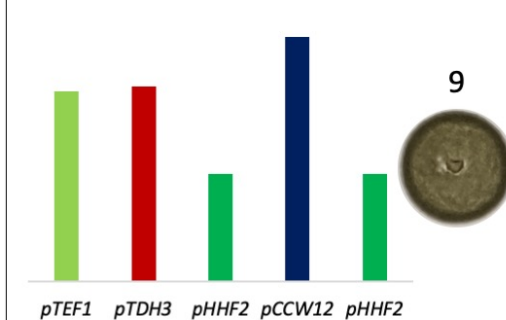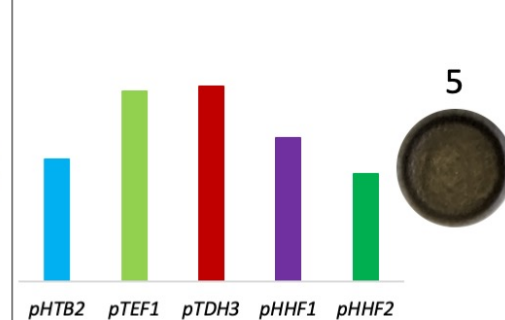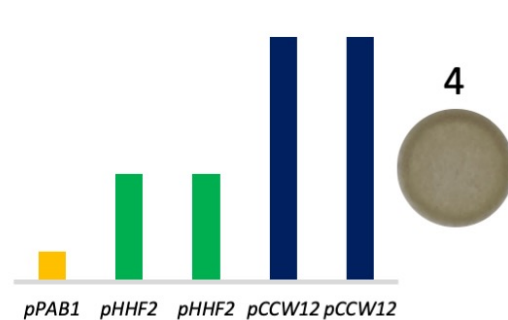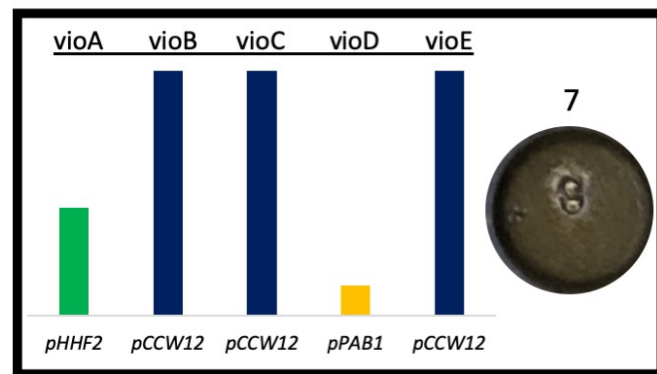
Figure S11. **Combinatorial assembly of violacein pathway assembly in *S. boulardii*.** Violacein pathway consisting of 5 genes (*vioA*, *vioB*, *vioC, vioD* and *vioE*) were assembled similar to β-carotene pathway. 8 out of 24 isolates (Supplementary Figure S8) were selected to proceed with sequencing based on stability of colony color after 3 serial passages. Sanger sequencing was done in a similar manner to the β-carotene isolates. Numbers on the colonies corresponds to the colony number from isolate plates on Figure S8c. The bar heights represent the normalized fluorescence values in linear scale for each promoter according to promoter characterization work (Figure 1a)
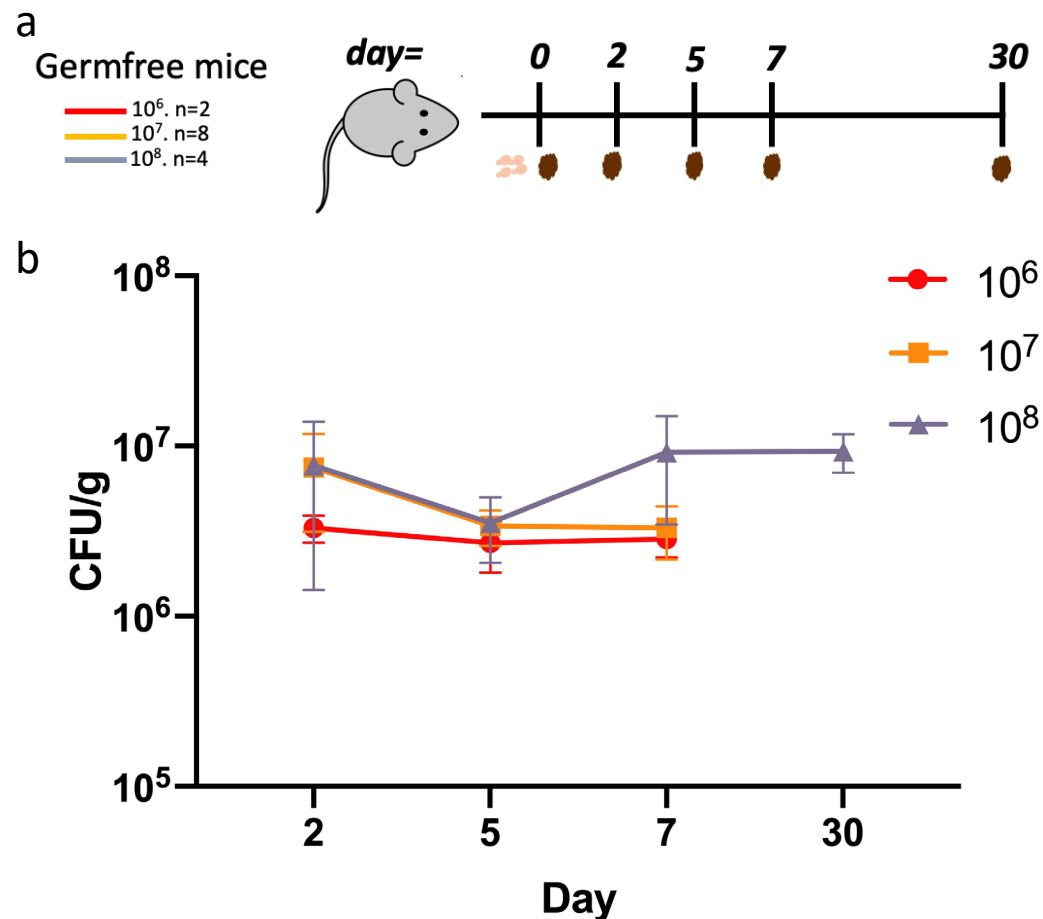
Figure S12. Dosage impacts the residence time of *S. boulardii* in germfree mice. **a**. germfree mice were gavaged with 3 different amounts of *S. boulardii* (10^6, 10^7 and 10^8 cells) on day 0. **b**. Residence time of *S. boulardii* in germfree mice. Fecal samples were collected as shown in the timeline. Error bars indicate the standard deviation observed among 2 germ free mice for 10^6 CFU treatment, 8 germ free mice for 10^7 CFU treatment, and 4 germ free mice for 10^8 CFU treatment In all mouse models. Feces were collected prior to Sb gavage during days when both occurred.
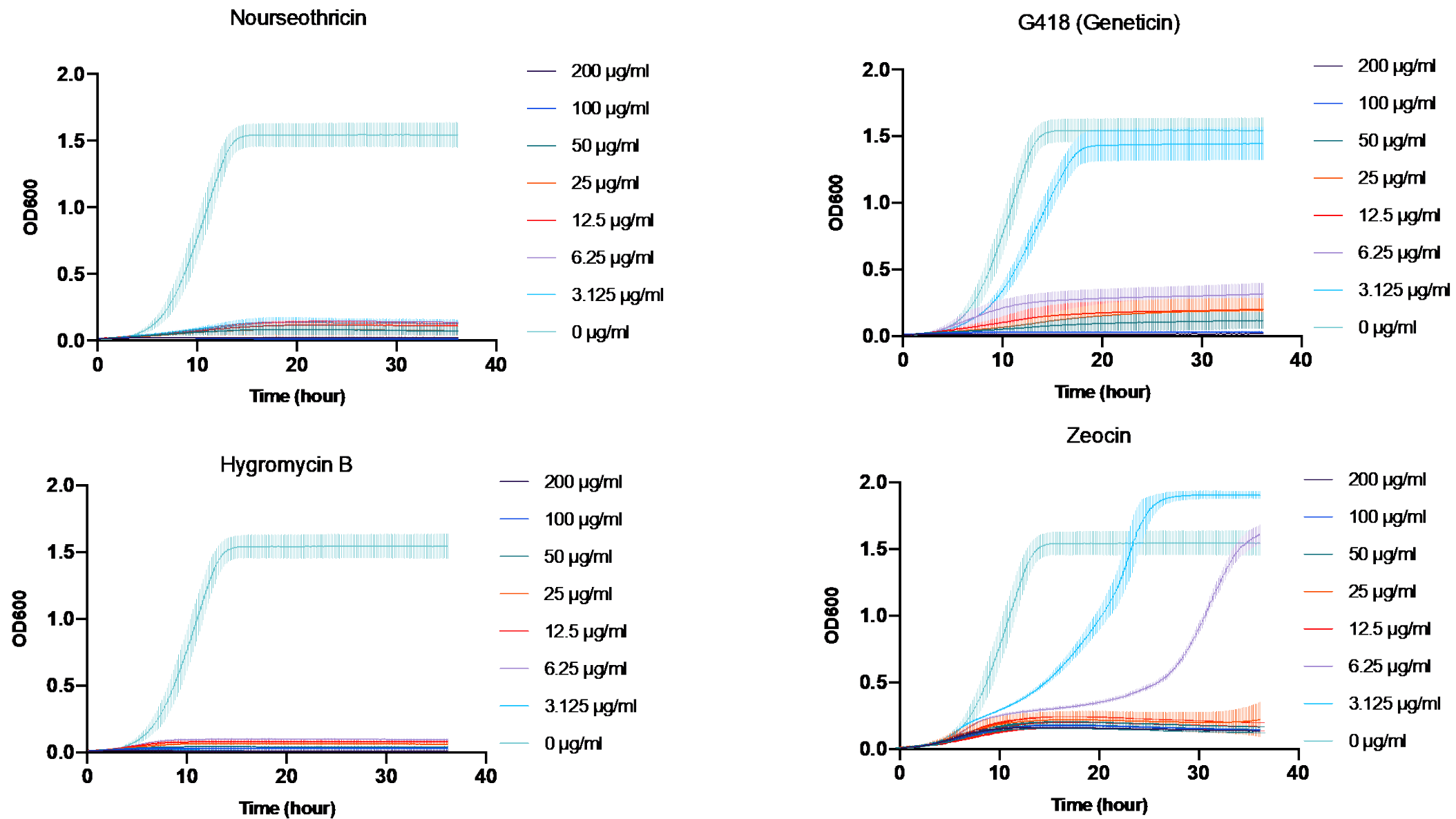
Figure S13. *S. boulardii* **Minimum Inhibitory Concentration (MIC) Tests with Nourseothricin, G418 Geneticin, Hygromycin B and Zeocin.** Error bars indicate the standard deviation observed among 3 biological replicates.

MoClo kit	Promoter	Score	Expect	Identities	Gaps
YTK009	pTDH3	1218 bits(659)	0	673/680(99%)	0/680(0%)
YTK010	pCCW12	1234 bits (668)	0	690/700 (98%)	4/700 (0%)
YTK011	pPGK1	1282 bits(694)	0	698/700(99%)	0/700(0%)
YTK012	pHHF2	1197 bits(648)	0	667/676(99%)	1/676(0%)
YTK013	pTEF1	1271 bits(688)	0	696/700(99%)	0/700(0%)
YTK014	pTEF2	917 bits(496)	0	534/550(97%)	11/550(2%)
YTK015	pHHF1	1254 bits(679)	0	694/701(99%)	1/701(0%)
YTK016	pHTB2	1210 bits(655)	0	683/696(98%)	4/696(0%)
YTK017	pRPL18B	1236 bits(669)	0	690/700(99%)	2/700(0%)
YTK018	pALD6	1266 bits(685)	0	695/700(99%)	0/700(0%)
YTK019	pPAB1	1271 bits(688)	0	697/701(99%)	1/701(0%)
YTK020	pRET2	1288 bits(697)	0	699/700(99%)	0/700(0%)
YTK021	pRNR1	1266 bits(685)	0	695/700(99%)	0/700(0%)
YTK022	pSAC6	1266 bits(685)	0	695/700(99%)	0/700(0%)
YTK023	pRNR2	1251 bits(677)	0	695/703(99%)	4/703(0%)
YTK024	pPOP6	1168 bits(632)	0	688/712(97%)	15/712(2%)
YTK025	pRAD27	1184 bits(641)	0	678/694(98%)	9/694(1%)
YTK026	pPSP2	1236 bits(669)	0	689/699(99%)	0/699(0%)
YTK027	pREV1	1251 bits(677)	0	693/700(99%)	4/700(0%)
YTK028	pMFA1	1271 bits(688)	0	697/701(99%)	1/701(0%)

Table S1. MoClo kit promoters blasted against *S.boulardii's* genome

Site	Chromosome	Locus
INT 1	V	YERCΔ8
INT 2	VIII	YHRCΔ14
INT 3	XV	non-coding region between NTR1(YOR071c) and GYP1 (YOR070c)
INT 4	XI	non-coding region between SRP40 (YKR092C) and PTR2 (YKR093W)
INT 5	XVI	YPRCτ3

Table S2. Integration locations (INT1-INT5) in *S. boulardii*'s genome.

INT site	SpCas9 guide	LbCpf1 guide
1	ACTCCTGGGAGAGAACATTC	TCTTCCTTCCCGTTATACTTTGT
	AACTAGTATACCATCATATA	ATAATTGTTCGGATTGCATTGTT
	AATTCACAAAAGAGAATCGA	TGAATTCCTATAACGTCGGGAGA
2	ACAAATGTCAGAAATATGGC	TCATACAACCAATGATTAATGTC
3	TATTAGAACCAGGGAGGTCC	AAAGATCCATACTTCTCTACATT
4	TTTCAACGCTTTCGAAGATG	TGTCAGATGTCATTATGGTCTCC
	GAATACTCAGACGTTTTCTG	CAGCCACATCTACAGGATGTTGA
	CAGAACCGTGACGCAATCTG	CCGGAAAAGCTAAGAGTTTTCTG
5	GGCTAATATAATGGTGATTC	GCAACCCAAGACTCGGCATACCA
	GATCAATATAACAATGCGTC	ACGTTTCCTTTTGCAATAGGTAC
	ACAGTGCTGAAGCAGAGATA	GAATATATCTCTCCAATACAGCG

Table S3. Guide RNA sequences used for genome editing assisted with the CRISPR nucleases SpCas9 or LbCas12a

a

	Genome Editing Method		
Site	SpCas9	LbCas12a	DNA
INT 1	191/232	399/424	34/72
	531/603	186/199	44/68
	237/275	397/401	21/58
INT 4	526/627	751/795	54/98
	588/679	743/784	62/81
	299/358	782/839	46/73
INT 5	503/597	679/716	19/92
	280/328	632/662	41/142
	242/294	729/764	38/107

b

	Genome Editing Method %		
Site	SpCas9	LbCas12a	DNA
INT 1	82.3	94.1	47.2
	88.1	93.5	64.7
	86.2	99.0	36.2
Avg INT 1	85.5	95.5	49.4
INT 4	83.9	94.5	55.1
	86.6	94.8	76.5
	83.5	93.2	63.0
Avg INT 4	84.7	94.1	64.9
INT 5	84.3	94.8	20.7
	85.4	95.5	28.9
	82.3	95.4	35.5
Avg INT 5	84.0	95.2	28.3

Table S4. *S. boulardii* genome editing efficiencies using 3 different methods. a. Number of colonies screened for each editing method. Successfully edited cells are defined by the number of fluorescent (mTurquoise2) colonies divided by the total number of colonies on the plate **b.** The percentage of successfully edited cells in the 3 different locations using 3 different editing methods.